Nonlinear Dyn (2024) 112:2453–2476
https://doi.org/10.1007/s11071-023-09178-z

ORIGINAL PAPER

Analytical and numerical stability analysis of a toroidal wheel with nonholonomic constraints

A. G. Agúndez · D. García-Vallejo · E. Freire

Received: 11 January 2023 / Accepted: 18 October 2023 / Published online: 26 December 2023

Abstract In this paper, a detailed and comprehensive linear stability analysis of a rolling toroidal wheel is performed. The wheel is modeled as a rigid toroid-shaped body rolling without slipping on a horizontal surface. The nonlinear equations of motion constitute a Differential-Algebraic Equations system, given by the dynamic equilibrium equations augmented with the nonholonomic constraints, which arise from the no-slip condition. The circular steady motion and the linearized equations of motion along this relative equilibrium are obtained, for both the solid and hollow tori. The expressions of the linearized equations and the corresponding eigenvalues are derived analytically as a function of the torus aspect ratio. The variation of the stability boundary with the torus aspect ratio is shown. A comparison of the results obtained in the solid and hollow scenarios is included, and all the results are validated with the rolling hoop, which corresponds to a degenerate torus with zero aspect ratio. In the particular case of the steady straight-line rolling and spinning about a vertical diameter, which constitute limit motions of the circular steady motion, the critical rotational and angular speeds required for stabilization are obtained.

Keywords Toroidal wheel · Nonholonomic systems · Linearization · Stability analysis

A. G. Agúndez (✉) · D. García-Vallejo
Department of Mechanical Engineering and Manufacturing, Universidad de Sevilla, Seville, Spain
e-mail: agarciaagundez@us.es

D. García-Vallejo
e-mail: dgvallejo@us.es

E. Freire
Department of Applied Mathematics II, Universidad de Sevilla, Seville, Spain
e-mail: efrem@us.es

1 Introduction

Nonholonomic systems are physical systems subject to constraints that involve both positions and velocities and are non-integrable. In contrast to classical Lagrangian or Hamiltonian systems, nonholonomic systems are nonvariational [1]. A classical example of nonholonomic system is a body with rolling contact, as a wheel rolling without slipping.

The interest in nonholonomic systems dates back to the late nineteenth century. After the incorrect application of the Lagrange equations in the presence of nonintegrable constraints, the equations of motion of a nonholonomic system were derived by Ferrers [2] in 1872. These equations were given in the form of Euler-Lagrange equations, including some additional terms arising from the constraints (but without Lagrange multipliers). Next, Voronetz performed, in 1901, the formal derivation of these equations [3]. Chaplygin obtained, for the case of cyclic configuration variables, the so-called Chaplygin equations [4,5], which engendered the technique of nonholonomic reduction. In his fundamental work Principles of Mechanics [6], Hertz first coined the term ‘nonholonomic’ and showed the inap-

plicability of variational principles and Lagrange equations to nonholonomic systems. The works of Borisov et al. [7], Bloch et al. [1] and Manuel de León [8] can be followed to find details about the development of nonholonomic mechanics.

The research on rolling bodies went hand in hand with the development of nonholonomic mechanics. The first known work devoted to the dynamics of a rolling rigid body is attributed to Euler [9], in which small oscillations of a body rolling without slipping were studied. The work of Poisson [10], which addresses the integrability of a heavy top moving on a smooth surface, gave rise to multiple papers investigating the integrability of the equations of motion of a disk rolling without slipping. Slesser [11] studied for the first time, in 1861, the motion of a rolling symmetrical disk on a horizontal rough plane. Vierkandt [12], in 1892, revealed that, on an appropriate symmetry-reduced space, all motions of the rolling disk are periodic. Chaplygin [13] showed the integrability of the rolling motion of an axisymmetric body on a horizontal plane. In the particular case of the rolling disk, the reduction of the problem to the analysis of hypergeometric quadratures was presented. Independently from Chaplygin, in 1900, Appel [14] and Korteweg [15] carried out the integration of the equations of motion of a disk with hyperelliptic functions, and Gallop [16] obtained the same results by resorting to Legendre functions. Furthermore, Carvallo [17] and Routh [18] studied the stability of the rolling disk, although these works did not include any information on the bifurcations of the system.

Other works devoted to analyse the stability of the steady motions of the rolling disk, taking advantage of the classical integrability results, are those of Mindlin [19,20], Duvakin [21] and Karapetyan [22]. Kolesnikov [23] and Fedorov [24] discussed qualitative properties of the disk motion, and Kozlov et al. [25] studied the nonintegrable problem of a disk moving on an inclined plane. O'Reilly [26] analysed the bifurcations and stability of the steady motions for both rolling and sliding disks, obtaining two-parameter families of integrable second-order differential equations. The results showed that the bifurcations of the steady motions of the disks are either of the pitchfork or saddle-node type. The study of bifurcations and stability of the disk's stationary motions was also performed by Cushman et al. [27] and Kuleshov [28]. Borisov et al. [29] showed different trajectories drawn by the contact point in the body-fixed and relative frames of references, and presented a complete three-dimensional bifurcation diagram in the space of the first integrals. Zenkov et al. [30] analysed, by using an energy-momentum analysis for nonholonomic systems, the stability of the relative equilibria of the rolling disk. Paris et al. [31] studied the circular rolling steady motion of the disk and derived the expression for the frequency of small oscillations about this reference motion. The book of Cushman et al. [32] provides a modern differential geometric treatment of linearly nonholonomically constrained systems and, in particular, analyzes the stability and the corresponding bifurcation diagram of the rolling disk. Moreover, a detailed linear stability analysis of the straight-line rolling, spinning about a vertical diameter and tumbling solutions of the rolling disk was presented by Przybylska [33]. The dynamics of an unbalanced disk with a single nonholonomic constraint was studied in a recent work by Kilin et al. [34]. In addition, there exist several works devoted to other nonholonomic rolling bodies. Borisov et al. [35] consider cases of existence of invariant measure, additional first integrals and Poisson structure in the problem of rigid body's rolling without sliding on a plane and a sphere. The particular examples of nonholonomic systems addressed in this work, in addition to the rolling disk, are: a dynamically symmetric ball with the displaced center of mass rolling on a plane; the rolling of balanced, dynamically nonsymmetric ball (Chaplygin ball); the rolling of an unbalanced, dynamically nonsymmetric ball on a plane and the rolling of an ellipsoid on a plane. Moreover, different examples of bodies rolling on a sphere are included in [35]: the problem of rolling of round disk; a ball with displaced center; a balanced, dynamically nonsymmetric ball on sphere; the unbalanced, dynamically nonsymmetric ball on sphere; and the rolling of body with partially flat surface on sphere. Other important works devoted to the rolling of a ball on different surfaces are those of Hennans [36] and Borisov et al. [37–40]. A recent work of Antali et al. [41] addresses the kinematics and dynamics of a rigid body in contact with two rigid surfaces in the presence of dry friction.

The nonholonomic rolling torus is a particular case of axisymmetric body of revolution rolling without slipping on a horizontal plane. The complete integrability, the corresponding reduction of order and the stability analysis of these bodies can be found in several works [13,35]. Nevertheless, the authors have not found a single work in the literature including a detailed

stability analysis of the relative equilibria of the rolling toroidal wheel in terms of the geometric parameters of the torus. Hauser and Saccon [42] presented the equations of motion of a torus with a general contact profile, which rolls without slipping and is actuated by drive and steer torques. A stability analysis, considering similar geometric and inertial parameters to those of a motorcycle tire, was performed. García-Agúndez et al. [43] studied the linear stability of the steady forward motion of a solid rolling torus. Moreover, some examples of nonholonomic multibody models of vehicles with toroidal wheels can be found [44–48].

The novelty of the present paper is the performance of a detailed and comprehensive stability analysis of the rolling toroidal wheel. The linear stability of the relative equilibria of the rolling torus is studied, which, to the best knowledge of the authors, has not been done in any previous work of the literature. The linearized equations of motion along the circular steady motion, the straight-line rolling and the spinning about a vertical diameter, and the corresponding eigenvalues, are obtained as a function of the torus geometric parameters. The results are entirely developed analytically and numerically supported. Furthermore, a comparison between the linear stability results of the solid and hollow rolling tori is presented. The results of the rolling toroidal wheel are validated and compared with those of the rolling hoop, which constitutes a degenerate torus. The nonlinear equations of motion are linearized along the circular steady motion by following a linearization procedure suitable for nonholonomic systems, which can be found in [49]. This methodology, despite not obtaining a minimal-sized Jacobian matrix and not fully exploiting the symmetry of the problem, allows for obtaining the stability results of the rolling torus in terms of its geometric parameters in a clear and straightforward way, being natural and recognizable for the mechanical engineering community. This proposed methodology has already been successfully used in complex multibody dynamics problems, to study the linear stability of the waveboard [48] or the bicycle [49].

The paper is structured as follows. Following the Introduction, Sect. 2 describes the toroidal wheel model and presents the nonlinear equations of motion. Next, Sect. 3 presents the circular steady motion and the linearized equations of motion along this reference solution. Section 4 shows all the results of the stability analysis. In particular, Sects. 4.1 and 4.2 present the linear stability analysis of the steady straight-line rolling motion and the spinning motion about a vertical diameter, respectively, and Sect. 4.3 includes the stability results of the circular steady motion. Finally, Sect. 5 summarizes the main conclusions drawn from the present work.

2 Description of the model and nonlinear equations of motion

In this section, the toroidal wheel model is described and the nonlinear equations of motion are presented.

2.1 Description of the model

The wheel is modeled as a rigid torus that rolls without slipping on a horizontal surface. The mechanical model consists of five generalized coordinates ($n = 5$), with the vector of coordinates $\boldsymbol{x} \in \mathbb{R}^n$ given by:

$$\boldsymbol{x} = \left(x_C \;\; y_C \;\; \psi \;\; \phi \;\; \theta \right)^{\mathrm{T}}, \tag{1}$$

where x_C and y_C locate the contact point C of the wheel with the ground, and ψ, ϕ and θ are the yaw, lean and roll angles, respectively. The global (inertial) frame is denoted as body 1 and the wheel is body 2. Figure 1 shows the generalized coordinates and the body frame of the toroidal wheel. To describe the orientation of the intermediate frames $\langle X'Y'Z' \rangle$, $\langle X''Y''Z'' \rangle$ and the body frame 2 $\langle X_2 Y_2 Z_2 \rangle$, depicted in Fig. 1, the matrices $\boldsymbol{R}^{'}$, $\boldsymbol{R}^{''}$ and $\boldsymbol{R}_2$ are defined. These matrices are computed by using the elemental rotation matrices $\boldsymbol{R}_\psi$, $\boldsymbol{R}_\phi$ and $\boldsymbol{R}_\theta$ as follows:

$$\boldsymbol{R}^{'}(\boldsymbol{x}) = \boldsymbol{R}_\psi,$$

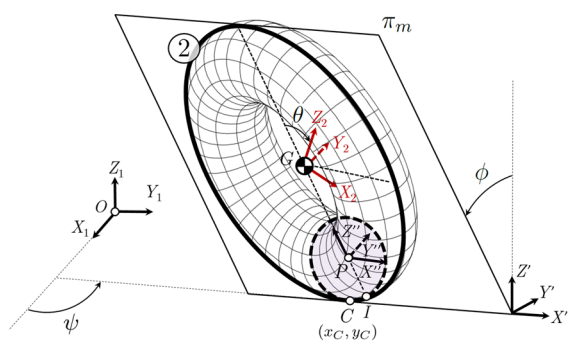

Fig. 1 Mechanical model of the toroidal wheel: generalized coordinates and body frames

$$\boldsymbol{R}^{''}(\boldsymbol{x}) = \boldsymbol{R}_{\psi}\boldsymbol{R}_{\phi},$$
$$\boldsymbol{R}_2(\boldsymbol{x}) = \boldsymbol{R}_{\psi}\boldsymbol{R}_{\phi}\boldsymbol{R}_{\theta}. \tag{2}$$

In this work, a circular cross-section of the toroidal wheel is considered. The toroidal geometry is defined by the torus aspect ratio η, which is computed as the ratio of the minor to the major radius of the torus, denoted as a and b, respectively:

$$\eta = \frac{a}{b}. \tag{3}$$

For a real torus, $a < b$ ($\eta < 1$) is required. In any case, the subsequent analysis is also valid for the limit cases $a > b$ (degenerate torus), $a = 0$ (hoop) and $b = 0$ (sphere).

The plane of symmetry π_m is the middle plane of the toroidal wheel and contains the hoop of equivalent radius R. The minor and major radii verify the following relation:

$$a + b = R. \tag{4}$$

Figure 2 shows a front view of the toroidal wheel, with the plane of symmetry π_m, the minor and major radii. In addition to the contact point C, other points of interest of the system are also depicted in Fig. 2. The centre of mass of the wheel is G, the centre of the torus tube is P and I is the lowest point of the hoop of equivalent radius. The position vectors of C and G, expressed in the global frame, are given by:

$$\boldsymbol{r}_C = \begin{pmatrix} x_C & y_C & 0 \end{pmatrix}^{\mathrm{T}}, \quad \boldsymbol{r}_G = \boldsymbol{r}_C + \boldsymbol{r}_{CP} + \boldsymbol{r}_{PG}, \tag{5}$$

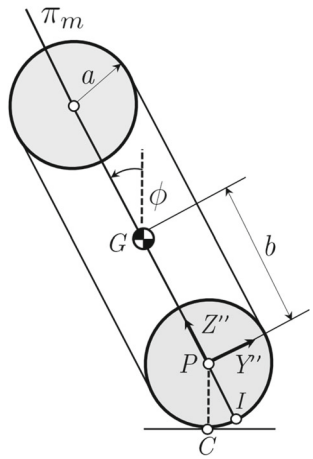

Fig. 2 Front view of the toroidal wheel

with

$$\boldsymbol{r}_{CP} = \begin{pmatrix} 0 & 0 & a \end{pmatrix}^{\mathrm{T}}, \qquad \boldsymbol{r}_{PG} = \boldsymbol{R}^{''}\bar{\boldsymbol{r}}_{PG}, \tag{6}$$

and $\bar{\boldsymbol{r}}_{PG} = \begin{pmatrix} 0 & 0 & b \end{pmatrix}^{\mathrm{T}}$.

The condition of rolling without slipping leads to two nonholonomic constraints ($l = 2$):

$$\boldsymbol{C}_{nh}(\boldsymbol{x}, \dot{\boldsymbol{x}}) = \boldsymbol{B}(\boldsymbol{x})\dot{\boldsymbol{x}} = \begin{pmatrix} v_{C_x} \\ v_{C_y} \end{pmatrix} = \begin{pmatrix} 0 \\ 0 \end{pmatrix}, \tag{7}$$

where $\boldsymbol{C}_{nh}(\boldsymbol{x}, \dot{\boldsymbol{x}})$ is the $l \times 1$ vector of nonholonomic constraints, linearly dependent on the generalized velocities; v_{C_x} and v_{C_y} are the X_1 and Y_1- components of the velocity of the contact point $\boldsymbol{v}_C$; and $\boldsymbol{B}(\boldsymbol{x})$ is a $l \times n$ matrix. Since the nonholonomic constraints are linear with respect to the system velocities, the matrix $\boldsymbol{B}(\boldsymbol{x})$ can be computed as:

$$\boldsymbol{B}(\boldsymbol{x}) = \frac{\partial \boldsymbol{C}_{nh}(\boldsymbol{x}, \dot{\boldsymbol{x}})}{\partial \dot{\boldsymbol{x}}}. \tag{8}$$

The velocity of the contact point $\boldsymbol{v}_C$ is given by:

$$\boldsymbol{v}_C = \boldsymbol{v}_G + \boldsymbol{\omega}_{21} \times \boldsymbol{r}_{GC}, \tag{9}$$

where $\boldsymbol{v}_G$ is the velocity of the centre of mass, $\boldsymbol{\omega}_{21}$ is the angular velocity of the wheel and $\boldsymbol{r}_{GC} = -(\boldsymbol{r}_{CP} + \boldsymbol{r}_{PG})$. The use of Eq. (9) leads to:

$$\boldsymbol{v}_C = \begin{pmatrix} v_{C_x} \\ v_{C_y} \\ v_{C_z} \end{pmatrix} = \begin{pmatrix} \dot{x}_C - (b + a\cos(\phi))\,\dot{\theta}\cos(\psi) - a\dot{\phi}\sin(\psi) \\ \dot{y}_C - (b + a\cos(\phi))\,\dot{\theta}\sin(\psi) + a\dot{\phi}\cos(\psi) \\ 0 \end{pmatrix}. \tag{10}$$

Note that, in Eq. (10), the Z-component of $\boldsymbol{v}_C$ is null and is therefore not included in the nonholonomic constraints (7). Since the wheel is described by using five coordinates ($n = 5$), the number of degrees of freedom of the system is three ($n_g = n - l = 3$).

2.2 Equations of motion

The equations of motion of the rolling toroidal wheel are given by the dynamic equilibrium equations, which are derived as explained in Schiehlen [50], augmented with the nonholonomic constraints (7), leading to the following index-2 Differential Algebraic Equations (DAE) system:

$$\boldsymbol{M}(\boldsymbol{x})\ddot{\boldsymbol{x}} + \boldsymbol{B}^{\mathrm{T}}(\boldsymbol{x})\boldsymbol{\Lambda} = \boldsymbol{Q}(\boldsymbol{x}, \dot{\boldsymbol{x}}), \tag{11}$$

$$\boldsymbol{C}_{nh}\left(\boldsymbol{x},\dot{\boldsymbol{x}}\right)=\boldsymbol{B}\left(\boldsymbol{x}\right)\dot{\boldsymbol{x}}=\boldsymbol{0}, \tag{12}$$

where $\boldsymbol{M}\left(\boldsymbol{x}\right)$ is the $n\times n$ mass matrix; $\boldsymbol{Q}\left(\boldsymbol{x},\dot{\boldsymbol{x}}\right)$ is the $n\times 1$ vector of generalized forces, and $\boldsymbol{\Lambda}$ is the $l\times 1$ vector of Lagrange multipliers. All the vectors and matrices in Eqs. (11) and (12) are smooth functions. The vector of generalized forces $\boldsymbol{Q}\left(\boldsymbol{x},\dot{\boldsymbol{x}}\right)$ can be expressed as:

$$\boldsymbol{Q}\left(\boldsymbol{x},\dot{\boldsymbol{x}}\right)=\boldsymbol{Q}_{g}\left(\boldsymbol{x}\right)+\boldsymbol{Q}_{v}\left(\boldsymbol{x},\dot{\boldsymbol{x}}\right), \tag{13}$$

where $\boldsymbol{Q}_{g}\left(\boldsymbol{x}\right)$ is the generalized gravity forces vector and $\boldsymbol{Q}_{v}\left(\boldsymbol{x},\dot{\boldsymbol{x}}\right)$ is the quadratic-velocity inertia term, associated with the inertia forces that are quadratic with respect to the system velocities (centrifugal and Coriolis forces). The expressions of the matrices $\boldsymbol{M}\left(\boldsymbol{x}\right)$, $\boldsymbol{B}\left(\boldsymbol{x}\right)$, and the vectors $\boldsymbol{Q}_{g}\left(\boldsymbol{x}\right)$, $\boldsymbol{Q}_{v}\left(\boldsymbol{x},\dot{\boldsymbol{x}}\right)$ are given by:

$$\begin{aligned}\boldsymbol{M}\left(\boldsymbol{x}\right)&=\begin{pmatrix} m & 0 & mb\cos(\psi)\sin(\phi) \\ 0 & m & mb\sin(\psi)\sin(\phi) \\ mb\cos(\psi)\sin(\phi) & mb\sin(\psi)\sin(\phi) & I_d^i+\left(I_p^i-I_d^i+mb^2\right)\sin^2(\phi) \\ mb\sin(\psi)\cos(\phi) & -mb\cos(\psi)\cos(\phi) & 0 \\ 0 & 0 & I_p^i\sin(\phi)\end{pmatrix}\\ &\quad\begin{pmatrix} mb\sin(\psi)\cos(\phi) & 0 \\ -mb\cos(\psi)\cos(\phi) & 0 \\ 0 & I_p^i\sin(\phi) \\ I_d^i+mb^2 & 0 \\ 0 & I_p^i\end{pmatrix},\end{aligned} \tag{14}$$

$$\boldsymbol{B}\left(\boldsymbol{x}\right)=\begin{pmatrix}1&0&0&-a\sin\left(\psi\right)&-\left(b+a\cos\left(\phi\right)\right)\cos\left(\psi\right)\\0&1&0&a\cos\left(\psi\right)&-\left(b+a\cos\left(\phi\right)\right)\sin\left(\psi\right)\end{pmatrix}, \tag{15}$$

$$\boldsymbol{Q}_{g}\left(\boldsymbol{x}\right)=\begin{pmatrix}0\\0\\0\\mgb\sin\left(\phi\right)\\0\end{pmatrix},\quad \boldsymbol{Q}_{v}\left(\boldsymbol{x},\dot{\boldsymbol{x}}\right)=\begin{pmatrix}mb\left(\dot{\psi}^2+\dot{\phi}^2\right)\sin\left(\psi\right)\sin\left(\phi\right)-2mb\dot{\psi}\dot{\phi}\cos\left(\psi\right)\cos\left(\phi\right)\\-mb\left(\dot{\psi}^2+\dot{\phi}^2\right)\cos\left(\psi\right)\sin\left(\phi\right)-2mb\dot{\psi}\dot{\phi}\sin\left(\psi\right)\cos\left(\phi\right)\\-I_p^i\dot{\phi}\dot{\theta}\cos\left(\phi\right)-\left(I_p^i-I_d^i+mb^2\right)\dot{\psi}\dot{\phi}\sin\left(2\phi\right)\\I_p^i\dot{\psi}\dot{\theta}\cos\left(\phi\right)+\left(I_p^i-I_d^i+mb^2\right)\dot{\psi}^2\sin\left(\phi\right)\cos\left(\phi\right)\\-I_p^i\dot{\psi}\dot{\phi}\cos\left(\phi\right)\end{pmatrix}. \tag{16}$$

In Eqs. (14) and (16), I_d^i and I_p^i are the moments of inertia about a diameter and a vertical axis perpendicular to the wheel centre, respectively. The superscript i in I_d^i and I_p^i is henceforth used to distinguish between the solid and hollow scenarios, with $i=\{s,h\}$. Tatum [51] provides the expressions of the moments of inertia of a solid and hollow torus with circular cross-section:

$$I_d^s=\frac{1}{8}m\left(5a^2+4b^2\right),\quad I_p^s=\frac{1}{4}m\left(3a^2+4b^2\right),$$

$$I_d^h=\frac{1}{4}m\left(5a^2+2b^2\right),\quad I_p^h=\frac{1}{2}m\left(3a^2+2b^2\right). \tag{17}$$

For the limit case $a\rightarrow 0$, Eq. (17) give back the moments of inertia of the well-known hoop case.

3 Methodology

The objective of this section is to describe the circular steady motion of the rolling toroidal wheel and obtain the linearized equations along this relative equilibrium, as a function of the torus geometric parameters. To this end, the linearization approach proposed in [49], which has been successfully used to perform the linear stability analysis of complex nonholonomic multibody systems as the bicycle or the waveboard [48], is employed. This methodology, despite not fully exploiting the symmetry of the problem and not obtaining a minimal-sized Jacobian matrix, allows for obtaining the stability results of the rolling torus in terms of its geometric parameters in a clear and straightforward way, being recognizable for the mechanical engineering community.

Nevertheless, in the context of nonholonomic mechanics, the use of reduction methods that allow for reducing the order of nonholonomic equations of motion, with the help of symmetries and first integrals, is widely extended. The works of Chaplygin [13] or Voronetz [52] already addressed the reduction of the equations of nonholonomic examples, and the term nonholonomic reduction was proposed in the work of Koiller [53]. A review of the problem of the constructive reduction of nonholonomic systems with symmetries was performed by Borisov and Mamaev [54]. The reduced equations of motion of an arbitrary body of revolution rolling on a plane were presented by Borisov and Mamaev [35] and applied to several nonholonomic examples [29,35]. Therefore, due to the importance in nonholonomic mechanics, the methodology followed in [35] is first summarized, outlining its main steps. The use of this reduction method exploits the symmetries of nonholonomic systems and allows for obtaining a minimal-sized Jacobian matrix.

3.1 Reduction method

The nonholonomic rolling torus is a particular case of axisymmetric body of revolution rolling without slipping on a horizontal plane. The complete integrability, the corresponding reduction of order and the stability analysis of these bodies can be found in the literature [13,29,35]. The main steps of the methodology followed in Borisov and Mamaev [35] are summarized below:

- Identify the symmetry group of the system. The symmetry group of the rolling torus is $G = SE(2) \times SO(2)$, where the first multiplier represents arbitrariness in the choice of a fixed coordinate system, and the second corresponds to the axial symmetry of the rolling body.
- Compute the reduced equations of motion. This symmetry group can be used to reduce the equations of motion of an arbitrary body of revolution, with tensor of inertia $\boldsymbol{I} = \mathrm{diag}(I_1, I_1, I_3)$, to an autonomous fourth-order system [35]. The reduced equations can be expressed in terms of the variable $z = \sin(\phi)$, with $z \in (-1, 1)$, and a set of variables $K_1, K_2, K_3 \in \mathbb{R}$, which are linearly expressed in terms of the angular velocity of the body. The detailed expressions of K_1, K_2 and K_3 can be found in Borisov and Mamaev [35], and the system of equations is given by:

$$\begin{aligned}
\dot{z} &= kK_3, \\
\dot{K}_1 &= -k\rho_i I_3 \left(1 - \left(\frac{f_2}{f_1}\right)'\right) K_2 K_3, \\
\dot{K}_2 &= -k\rho_i m f_1 \left(f_1 - f_2'\right) K_1 K_3, \\
\dot{K}_3 &= k\left(A(z) K_1^2 + B(z) K_1 K_2\right) \\
&\quad + C(z) K_2^2 - \frac{\partial U(z)}{\partial z}.
\end{aligned} \tag{18}$$

  In Eq. (18), f_1 and f_2 are functions of z that define the surface of the body; U is the potential energy; the expressions of k, $A(z)$, $B(z)$ and $C(z)$ can be found in Borisov and Mamaev [35]; and ρ_i is the density of invariant measure, computed as:

$$\rho_i = \frac{1}{\sqrt{I_1 I_3 + m I_1 f_1^2 \left(1 - z^2\right) + m I_3 f_2^2}}. \tag{19}$$

- Computation of the relative equilibria. The relative equilibria correspond to the fixed points of the system of equations (18), which are given by the following pair of equations:

$$\begin{aligned}
&K_3 = 0, \\
&A(z) K_1^2 + B(z) K_1 K_2 + C(z) K_2^2 - \frac{\partial U(z)}{\partial z} = 0.
\end{aligned} \tag{20}$$

  From Eq. (18), given $z = z_0$, then K_1 and K_2 satisfy a quadratic equation.
- Linearization of the reduced equations. Let $z = z_0$, with $|z_0| < 1$, $K_1 = K_1^0$, $K_2 = K_2^0$ and $K_3 = 0$ define a relative equilibrium of the system (18). The linearization of Eq. (18) along this reference solution yields a 4×4 time-independent Jacobian matrix.
- Stability analysis of the reference solutions. The orbital stability of the reference solutions investigated in this work is defined by the stability of the fixed points of the system (18). Since the 4×4 Jacobian matrix does not depend explicitly on time and presents constant coefficients, the linear stability can be assessed directly by analyzing the set of eigenvalues of the time-independent matrix. The conservation laws of the system can be used to study the nonlinear stability of these solutions.

This methodology can be applied to the rolling toroidal wheel in the same manner as in previous works devoted to the rolling disk [29] or other rolling

bodies on a plane [35]. Despite the low dimension and high symmetry of the system being leveraged by this reduction method, the present work conducts the linear stability analysis of the rolling toroidal wheel using the linearization approach presented in Ref. [49]. This approach constitutes a powerful general-purpose methodology that, while not resulting in a minimal-sized Jacobian matrix, enables the derivation of explicit results regarding the system's stability.

3.2 Description of the circular steady motion

The nonlinear equations of motion (11)–(12) are linearized with respect to the circular steady motion of the toroidal wheel. The steady straight-line rolling motion and spinning about a vertical diameter, whose stability will also be studied in this work, are limit motions of the circular steady solution. A circular trajectory of radius ρ, described by the contact point C with a constant angular speed ω, can be expressed as:

$$\boldsymbol{x}^0(t) = \left(x_C^0(t)\ y_C^0(t)\ \psi^0(t)\ \phi^0(t)\ \theta^0(t)\right)^{\mathrm{T}}, \quad (21)$$

with

$$\begin{aligned} x_C^0(t) &= \rho\cos(\omega t), & y_C^0(t) &= \rho\sin(\omega t), \\ \psi^0(t) &= \frac{\pi}{2} + \omega t, & \phi^0(t) &= \phi_0, \\ \theta^0(t) &= \Omega t, \end{aligned} \quad (22)$$

where Ω is the rotational speed of the wheel. Note that, in Eq. (22), $x_C^0(t)$ and $y_C^0(t)$ vary sinusoidally with time; the yaw angle $\psi^0(t)$ and the roll angle $\theta^0(t)$ grow linearly with time, and the lean angle $\phi^0(t)$ is constant throughout the circular steady motion and is denoted as ϕ_0.

The angular velocity ω and the rotational speed Ω are related by means of the nonholonomic constraints. Combining the nonholonomic constraints (7), the following expression is obtained for $\dot{\theta}$:

$$\dot{\theta} = \frac{\dot{x}_C\cos(\psi) + \dot{y}_C\sin(\psi)}{R\cos(\phi)}. \quad (23)$$

Particularizing Eq. (23) for the reference solution (22), the following relation is obtained:

$$\omega = \left(\frac{b + a\cos(\phi_0)}{\rho}\right)\Omega. \quad (24)$$

A characteristic time of the torus system τ_0, related to free fall, and the angular frequency ω_0 are defined as follows:

$$\tau_0 = \sqrt{\frac{a+b}{g}}, \qquad \omega_0 = \frac{1}{\tau_0} = \sqrt{\frac{g}{a+b}}. \quad (25)$$

The following nondimensional angular and rotational velocities are introduced:

$$\bar{\omega} = \frac{\omega}{\omega_0}, \qquad \bar{\Omega} = \frac{\Omega}{\omega_0}. \quad (26)$$

To satisfy the equilibrium equations (11), the lean angle ϕ_0 of Eq. (22) verifies:

$$\begin{aligned} &\bar{\omega}^2\sin(\phi_0)\left(\left(\eta^2+12\right)\cos(\phi_0)+8\eta\right) \\ &\quad + 8(1+\eta)\sin(\phi_0) + \bar{\Omega}\bar{\omega}\left(\left(14\eta^2+16\right)\cos(\phi_0)\right) \\ &\quad + 4\eta(3+\cos(2\phi_0)) = 0, \end{aligned} \quad (27)$$

$$\begin{aligned} &\bar{\omega}^2\sin(\phi_0)\left(\left(2\eta^2+12\right)\cos(\phi_0)+8\eta\right) \\ &\quad + 8(1+\eta)\sin(\phi_0) + \bar{\Omega}\bar{\omega}\left(\left(20\eta^2+16\right)\cos(\phi_0)\right) \\ &\quad + 4\eta(3+\cos(2\phi_0)) = 0, \end{aligned} \quad (28)$$

with $-\pi/2 < \phi_0 < 0$. Equations (27) and (28) correspond to the solid and hollow case, respectively. Note that Eqs. (27) and (28) also hold for the steady straight-line rolling and the spinning motion around a vertical diameter. In the case of the steady straight-line rolling, which corresponds to $\bar{\omega} \to 0$, Eqs. (27) and (28) yield $\phi_0 \to 0$. The same result is obtained when Eqs. (27) and (28) are particularized for the steady spinning around a vertical diameter, corresponding to $\bar{\Omega} \to 0$. In addition, Eqs. (27) and (28) can be particularized for the limit case $\eta \to 0$, to obtain the same equilibrium equation of the rolling hoop:

$$\begin{aligned} &\left(3\bar{\omega}^2\cos(\phi_0)+2\right)\tan(\phi_0) + 4\bar{\omega}\bar{\Omega} = 0, \\ &\text{with } -\pi/2 < \phi_0 < 0. \end{aligned} \quad (29)$$

Figures 3 and 4 show an arbitrary position of the rolling toroidal wheel and the rolling hoop, respectively, during the circular steady motion.

3.3 Linearization of the equations of motion

Consider the circular steady motion $\boldsymbol{x}^0(t)$ defined in Eqs. (21) and (22) and its time derivatives $\dot{\boldsymbol{x}}^0(t)$, $\ddot{\boldsymbol{x}}^0(t)$. This motion represents a known reference solution of

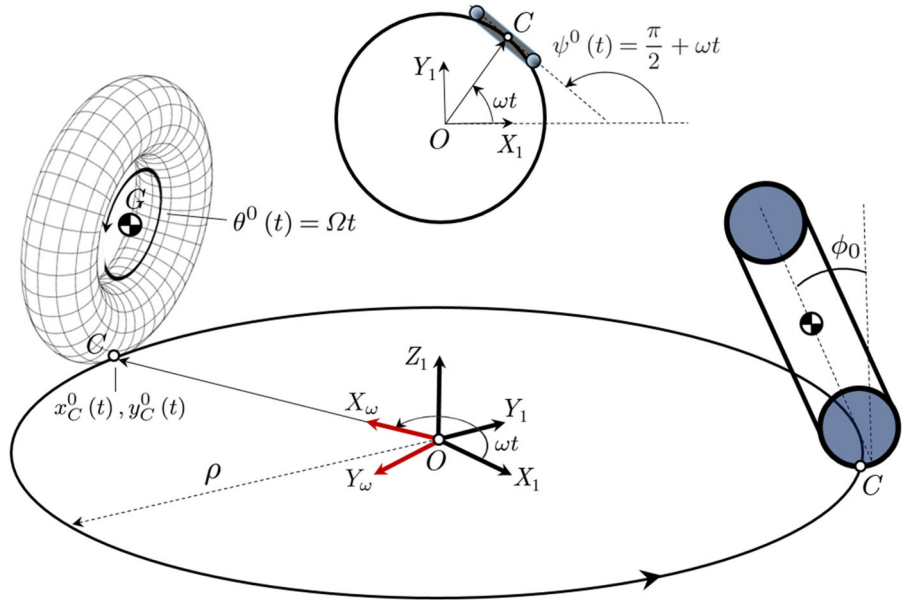

Fig. 3 Circular steady motion of the rolling toroidal wheel

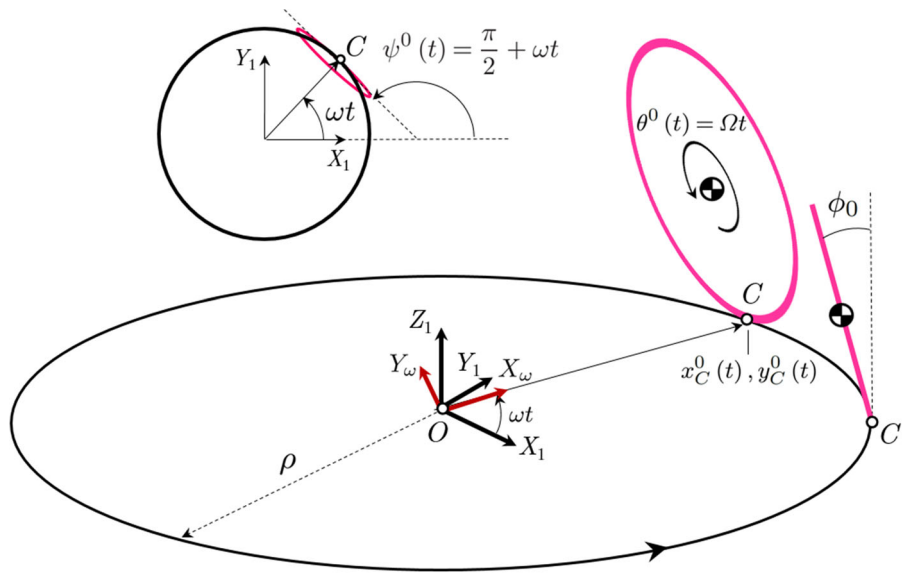

Fig. 4 Circular steady motion of the rolling hoop

the Differential-Algebraic Equations system given by Eqs. (11) and (12), and therefore verifies:

$$\boldsymbol{M}\left(\boldsymbol{x}^0\right)\ddot{\boldsymbol{x}}^0 + \boldsymbol{B}^{\mathrm{T}}\left(\boldsymbol{x}^0\right)\boldsymbol{\Lambda}^0 = \boldsymbol{Q}\left(\boldsymbol{x}^0, \dot{\boldsymbol{x}}^0\right), \tag{30}$$

$$\boldsymbol{C}_{nh}\left(\boldsymbol{x}^0, \dot{\boldsymbol{x}}^0\right) = \boldsymbol{B}\left(\boldsymbol{x}^0\right)\dot{\boldsymbol{x}}^0 = \boldsymbol{0}, \tag{31}$$

where $\boldsymbol{\Lambda}^0$ is the vector of Lagrange multipliers in the circular steady motion. The set $\boldsymbol{\Lambda}^0$ can be obtained from Eq. (30), which leads to:

$$\boldsymbol{\Lambda}^0(t) = \left(\Lambda_1^0(t)\ \Lambda_2^0(t)\right)^{\mathrm{T}}, \tag{32}$$

with $\Lambda_1^0(t) = m\omega^2(\rho + b\sin(\phi_0))\cos(\omega t)$ and $\Lambda_2^0(t) = m\omega^2(\rho + b\sin(\phi_0))\sin(\omega t)$. Note that $\Lambda_1^0(t)$ and $\Lambda_2^0(t)$ vary sinusoidally with time.

The variations $\tilde{\boldsymbol{x}}$, $\dot{\tilde{\boldsymbol{x}}}$, $\ddot{\tilde{\boldsymbol{x}}}$ and $\tilde{\boldsymbol{\Lambda}}$ with respect to the reference solution are introduced:

$$\tilde{\boldsymbol{x}} = \boldsymbol{x} - \boldsymbol{x}^0,\ \dot{\tilde{\boldsymbol{x}}} = \dot{\boldsymbol{x}} - \dot{\boldsymbol{x}}^0,$$
$$\ddot{\tilde{\boldsymbol{x}}} = \ddot{\boldsymbol{x}} - \ddot{\boldsymbol{x}}^0 \text{ and } \tilde{\boldsymbol{\Lambda}} = \boldsymbol{\Lambda} - \boldsymbol{\Lambda}^0. \tag{33}$$

A coordinate partition, based on $n-l$ independent and l dependent velocities, denoted as $\dot{\tilde{\boldsymbol{x}}}_{ai}$ and $\dot{\tilde{\boldsymbol{x}}}_{ad}$, respectively, is used: $\dot{\tilde{\boldsymbol{x}}} = \left(\dot{\tilde{\boldsymbol{x}}}_{ai}\ \dot{\tilde{\boldsymbol{x}}}_{ad}\right)^{\mathrm{T}}$. Similarly, the same partition at position level is considered: $\tilde{\boldsymbol{x}} = \left(\tilde{\boldsymbol{x}}_{ai}\ \tilde{\boldsymbol{x}}_{ad}\right)^{\mathrm{T}}$. In the case of the rolling toroidal wheel, $n=5$ and $l=2$. Choosing as independent coordinates the yaw, lean and roll angles ψ, ϕ and θ, the vectors of independent and dependent coordinates $\tilde{\boldsymbol{x}}_{ai}$ and $\tilde{\boldsymbol{x}}_{ad}$ are given by:

$$\tilde{\boldsymbol{x}}_{ai} = \left(\tilde{\psi}\ \tilde{\phi}\ \tilde{\theta}\right)^{\mathrm{T}}, \qquad \tilde{\boldsymbol{x}}_{ad} = \left(\tilde{x}_C\ \tilde{y}_C\right)^{\mathrm{T}}. \tag{34}$$

Following the linearization procedure presented in [49], which allows the computation of the reduced linearized equations of motion of a mechanical system with holonomic and nonholonomic constraints, the following linear ODE system is obtained:

$$\ddot{\tilde{\boldsymbol{x}}}_{ai} = \boldsymbol{J}_{21}\tilde{\boldsymbol{x}}_{ai} + \boldsymbol{J}_{22}\dot{\tilde{\boldsymbol{x}}}_{ai} + \boldsymbol{J}_{23}\tilde{\boldsymbol{x}}_{ad}, \tag{35}$$

$$\dot{\tilde{\boldsymbol{x}}}_{ad} = \boldsymbol{J}_{31}\tilde{\boldsymbol{x}}_{ai} + \boldsymbol{J}_{32}\dot{\tilde{\boldsymbol{x}}}_{ai} + \boldsymbol{J}_{33}\tilde{\boldsymbol{x}}_{ad}. \tag{36}$$

The computation of the matrices $\boldsymbol{J}_{21}$, $\boldsymbol{J}_{22}$, $\boldsymbol{J}_{23}$, $\boldsymbol{J}_{31}$, $\boldsymbol{J}_{32}$ and $\boldsymbol{J}_{33}$ in Eqs. (35) and (36) is developed in detail in [49]. Note that Eq. (35) represents the reduced linearized dynamic equations, and Eq. (36) corresponds to the linearized nonholonomic constraints.

The linearized equations of motion (35) and (36) can be written as a first order system by defining $\tilde{\boldsymbol{X}} = \left(\tilde{\boldsymbol{x}}_{ai}\ \dot{\tilde{\boldsymbol{x}}}_{ai}\ \tilde{\boldsymbol{x}}_{ad}\right)^{\mathrm{T}}$:

$$\dot{\tilde{\boldsymbol{X}}} = \boldsymbol{J}\tilde{\boldsymbol{X}}, \tag{37}$$

where $\boldsymbol{J}$ is the Jacobian matrix of the system, built as follows:

$$\boldsymbol{J} = \left(\begin{array}{c|c|c} \boldsymbol{0}_{(n-l)} & \boldsymbol{I}_{(n-l)} & \boldsymbol{0}_{(n-l)\times l} \\ \hline \boldsymbol{J}_{21} & \boldsymbol{J}_{22} & \boldsymbol{J}_{23} \\ \hline \boldsymbol{J}_{31} & \boldsymbol{J}_{32} & \boldsymbol{J}_{33} \end{array}\right). \tag{38}$$

In Eq. (38), $\boldsymbol{0}_{(n-l)}$ and $\boldsymbol{0}_{(n-l)\times l}$ are $(n-l)\times(n-l)$ and $(n-l)\times l$ null matrices, respectively, and $\boldsymbol{I}_{(n-l)}$ is the identity matrix of size $n-l$. Note that the size of $\boldsymbol{J}$ is $(2n-l)\times(2n-l) = 8\times 8$.

With the coordinate partition (34), the Jacobian matrix of Eq. (38), particularized for the circular steady motion (22), is obtained:

$$\boldsymbol{J}(t) = \left(\begin{array}{ccc|c|ccc|cc} 0 & 0 & 0 & 1 & 0 & 0 & 0 & 0 \\ 0 & 0 & 0 & 0 & 1 & 0 & 0 & 0 \\ 0 & 0 & 0 & 0 & 0 & 1 & 0 & 0 \\ \hline 0 & 0 & 0 & 0 & \alpha_1^i & 0 & 0 & 0 \\ 0 & \alpha_2^i & 0 & \alpha_3^i & 0 & \alpha_4^i & 0 & 0 \\ 0 & 0 & 0 & 0 & \alpha_5^i & 0 & 0 & 0 \\ \hline -\varrho\Omega\cos(\omega t) & a\Omega\sin(\phi_0)\sin(\omega t) & 0 & 0 & a\cos(\omega t) & -\varrho\sin(\omega t) & 0 & 0 \\ -\varrho\Omega\sin(\omega t) & -a\Omega\sin(\phi_0)\cos(\omega t) & 0 & 0 & a\sin(\omega t) & \varrho\cos(\omega t) & 0 & 0 \end{array}\right), \tag{39}$$

where $\varrho = b + a\cos(\phi_0)$ and the coefficients α_j^i, with $i = \{s, h\}$ and $j = 1\ldots 5$, are functions of the rotational speed Ω, the angular speed ω, the lean equilibrium angle ϕ_0 and the torus aspect ratio η:

$$\begin{aligned} \alpha_1^i(\Omega,\omega,\eta,\phi_0) &= \delta_1^i(\eta,\phi_0)\,\omega + \delta_2^i(\eta,\phi_0)\,\Omega, \\ \alpha_2^i(\Omega,\omega,\eta,\phi_0) &= \delta_3^i(\eta,\phi_0)\,\omega^2 + \delta_4^i(\eta,\phi_0)\,\frac{g}{R} \\ &\quad + \delta_5^i(\eta,\phi_0)\,\Omega\omega, \\ \alpha_3^i(\Omega,\omega,\eta,\phi_0) &= \delta_6^i(\eta,\phi_0)\,\omega + \delta_7^i(\eta,\phi_0)\,\Omega, \\ \alpha_4^i(\Omega,\omega,\eta,\phi_0) &= \delta_7^i(\eta,\phi_0)\,\omega, \\ \alpha_5^i(\Omega,\omega,\eta,\phi_0) &= \delta_8^i(\eta,\phi_0)\,\omega + \delta_9^i(\eta,\phi_0)\,\Omega. \end{aligned} \tag{40}$$

The analytical expressions of the functions $\delta_k^i(\eta,\phi_0)$ in Eq. (40), with $i = \{s, h\}$ and $k = 1\ldots 9$, can be found in "Appendix A", for both the solid and hollow scenarios.

3.4 Computation of the time-independent Jacobian matrix

Since the Jacobian matrix $\boldsymbol{J}(t)$ of Eq. (39) depends explicitly on time, the linear stability cannot be assessed directly by computing the set of eigenvalues of the Jacobian matrix. To eliminate the time-dependence from the Jacobian matrix, a coordinate transformation is

used. The transformation is based on the use of a rotating coordinate system $\langle X_\omega Y_\omega Z_\omega \rangle$ (see Fig. 3), which rotates with the toroidal wheel. Therefore, the following transformation can be defined:

$$\boldsymbol{x}\,(t) = \boldsymbol{A}\,(t)\,\bar{\boldsymbol{x}} + \boldsymbol{C}\,(t)\,, \tag{41}$$

where $\bar{\boldsymbol{x}}$ is the new vector of coordinates, associated with the rotating frame:

$$\bar{\boldsymbol{x}} = \left(\bar{x}_C\ \bar{y}_C\ \bar{\psi}\ \bar{\phi}\ \bar{\theta}\right)^{\mathrm{T}}. \tag{42}$$

In Eq. (41), the expressions of the transformation matrix $\boldsymbol{A}\,(t)$ and vector $\boldsymbol{C}\,(t)$ are:

$$\boldsymbol{A}\,(t) = \left(\begin{array}{c|c} \boldsymbol{L}\,(t) & \boldsymbol{0}_{2\times 3} \\ \hline \boldsymbol{0}_{3\times 2} & \boldsymbol{I}_{3\times 3} \end{array}\right), \text{ with}$$

$$\boldsymbol{L}(t) = \begin{pmatrix} \cos(\omega t) & -\sin(\omega t) \\ \sin(\omega t) & \cos(\omega t) \end{pmatrix}, \tag{43}$$

$$\boldsymbol{C}\,(t) = \left(0\ 0\ \omega t\ 0\ \Omega t\right)^{\mathrm{T}}. \tag{44}$$

Due to the symmetry of the circular steady motion (22), this reference solution can be expressed, in the rotating frame, as the following constant vector:

$$\bar{\boldsymbol{x}}^0 = \left(\bar{x}_C^0\ \bar{y}_C^0\ \bar{\psi}^0\ \bar{\phi}^0\ \bar{\theta}^0\right)^{\mathrm{T}} = \left(\rho\ 0\ \pi/2\ \phi_0\ 0\right)^{\mathrm{T}}. \tag{45}$$

In the same way, the Lagrange multipliers, expressed in the rotating frame, are denoted as $\boldsymbol{\Gamma}^0$ and verify:

$$\boldsymbol{\Lambda}^0 = \boldsymbol{L}\,(t)\,\boldsymbol{\Gamma}^0, \tag{46}$$

where the matrix $\boldsymbol{L}(t)$ was defined in Eq. (43). The use of Eqs. (32) and (46) yields:

$$\boldsymbol{\Gamma}^0 = \left(\Gamma_1^0\ \Gamma_2^0\right)^{\mathrm{T}} = \left(m\omega^2\,(\rho + R\sin(\phi_0))\ 0\right)^{\mathrm{T}}. \tag{47}$$

Note that, in contrast to the Lagrange multipliers $\boldsymbol{\Lambda}^0$ of Eq. (32), $\boldsymbol{\Gamma}^0$ is a constant vector.

Using that, from Eq. (33), $\boldsymbol{x} = \boldsymbol{x}^0 + \tilde{\boldsymbol{x}}$; from Eq. (41), $\boldsymbol{x}^0 = \boldsymbol{A}(t)\bar{\boldsymbol{x}}^0 + \boldsymbol{C}(t)$; and defining $\tilde{\bar{\boldsymbol{x}}} = \bar{\boldsymbol{x}} - \bar{\boldsymbol{x}}^0$, the following relation is found:

$$\tilde{\boldsymbol{x}} = \boldsymbol{A}(t)\tilde{\bar{\boldsymbol{x}}}. \tag{48}$$

Using the coordinate partition of Eq. (34), and the definition of the matrix $\boldsymbol{A}\,(t)$ in Eq. (43), Eq. (48) can be expressed as:

$$\begin{pmatrix} \tilde{\boldsymbol{x}}_{ad} \\ \tilde{\boldsymbol{x}}_{ai} \end{pmatrix} = \left(\begin{array}{c|c} \boldsymbol{L}\,(t) & \boldsymbol{0}_{2\times 3} \\ \hline \boldsymbol{0}_{3\times 2} & \boldsymbol{I}_{3\times 3} \end{array}\right) \begin{pmatrix} \tilde{\bar{\boldsymbol{x}}}_{ad} \\ \tilde{\bar{\boldsymbol{x}}}_{ai} \end{pmatrix}, \tag{49}$$

where $\tilde{\bar{\boldsymbol{x}}}_{ai} = \left(\tilde{\bar{\psi}}\ \tilde{\bar{\phi}}\ \tilde{\bar{\theta}}\right)^{\mathrm{T}}$ and $\tilde{\bar{\boldsymbol{x}}}_{ad} = \left(\tilde{\bar{x}}_C\ \tilde{\bar{y}}_C\right)^{\mathrm{T}}$. Differentiating with respect to time Eq. (49), the following relations at velocity level are obtained:

$$\dot{\tilde{\boldsymbol{x}}}_{ad} = \dot{\boldsymbol{L}}\,(t)\,\tilde{\bar{\boldsymbol{x}}}_{ad} + \boldsymbol{L}(t)\dot{\tilde{\bar{\boldsymbol{x}}}}_{ad}, \tag{50}$$

$$\dot{\tilde{\boldsymbol{x}}}_{ai} = \dot{\tilde{\bar{\boldsymbol{x}}}}_{ai}. \tag{51}$$

The substitution of Eqs. (50) and (51) in the linear system of equations (35) and (36) leads to:

$$\ddot{\tilde{\bar{\boldsymbol{x}}}}_{ai} = \bar{\boldsymbol{J}}_{21}\tilde{\bar{\boldsymbol{x}}}_{ai} + \bar{\boldsymbol{J}}_{22}\dot{\tilde{\bar{\boldsymbol{x}}}}_{ai} + \bar{\boldsymbol{J}}_{23}\tilde{\bar{\boldsymbol{x}}}_{ad}, \tag{52}$$

$$\dot{\tilde{\bar{\boldsymbol{x}}}}_{ad} = \bar{\boldsymbol{J}}_{31}\tilde{\bar{\boldsymbol{x}}}_{ai} + \bar{\boldsymbol{J}}_{32}\dot{\tilde{\bar{\boldsymbol{x}}}}_{ai} + \bar{\boldsymbol{J}}_{33}\tilde{\bar{\boldsymbol{x}}}_{ad}, \tag{53}$$

where the matrices $\bar{\boldsymbol{J}}_{21}$, $\bar{\boldsymbol{J}}_{22}$, $\bar{\boldsymbol{J}}_{23}$, $\bar{\boldsymbol{J}}_{31}$, $\bar{\boldsymbol{J}}_{32}$ and $\bar{\boldsymbol{J}}_{33}$ are computed as follows:

$$\begin{aligned} \bar{\boldsymbol{J}}_{21} &= \boldsymbol{J}_{21}, & \bar{\boldsymbol{J}}_{31} &= \boldsymbol{L}^{-1}\boldsymbol{J}_{31}, \\ \bar{\boldsymbol{J}}_{22} &= \boldsymbol{J}_{22}, & \bar{\boldsymbol{J}}_{32} &= \boldsymbol{L}^{-1}\boldsymbol{J}_{32}, \\ \bar{\boldsymbol{J}}_{23} &= \boldsymbol{J}_{23}\boldsymbol{L}, & \bar{\boldsymbol{J}}_{33} &= \boldsymbol{L}^{-1}\left(\boldsymbol{J}_{33}\boldsymbol{L} - \dot{\boldsymbol{L}}\right). \end{aligned} \tag{54}$$

Finally, defining $\tilde{\bar{\boldsymbol{X}}} = \left(\tilde{\bar{\boldsymbol{x}}}_{ai}\ \dot{\tilde{\bar{\boldsymbol{x}}}}_{ai}\ \tilde{\bar{\boldsymbol{x}}}_{ad}\right)^{\mathrm{T}}$, the linearized equations of motion (52) and (53) can be written as a first order system of the form $\dot{\tilde{\bar{\boldsymbol{X}}}} = \bar{\boldsymbol{J}}\tilde{\bar{\boldsymbol{X}}}$, with the Jacobian matrix $\bar{\boldsymbol{J}}$:

$$\bar{\boldsymbol{J}} = \left(\begin{array}{ccc|ccc|cc} 0 & 0 & 0 & 1 & 0 & 0 & 0 & 0 \\ 0 & 0 & 0 & 0 & 1 & 0 & 0 & 0 \\ 0 & 0 & 0 & 0 & 0 & 1 & 0 & 0 \\ \hline 0 & 0 & 0 & 0 & \alpha_1^i & 0 & 0 & 0 \\ 0 & \alpha_2^i & 0 & \alpha_3^i & 0 & \alpha_4^i & 0 & 0 \\ 0 & 0 & 0 & 0 & \alpha_5^i & 0 & 0 & 0 \\ \hline -\varrho\Omega & 0 & 0 & 0 & a & 0 & 0 & \omega \\ 0 & -a\Omega\sin(\phi_0) & 0 & 0 & 0 & \varrho & -\omega & 0 \end{array}\right), \tag{55}$$

where the coefficients α_j^i were defined in Eq. (40). Note that, in contrast to Eq. (39), the Jacobian matrix $\bar{\boldsymbol{J}}$ does not depend explicitly on time and presents constant coefficients. In this case, the linear stability can be assessed directly, being all the information contained in the set of eigenvalues of $\bar{\boldsymbol{J}}$.

The 8×8 Jacobian matrix (55) results in $2n - l = 8$ eigenvalues. As detailed in Ref. [49], the linearization approach yields $l = 2$ spurious eigenvalues, associated with the linearized nonholonomic constraints in Eq. (55). These eigenvalues are easily recognizable and, in this case, are given by $\pm\omega i$, aris-

ing from the rotating coordinate system $\langle X_\omega Y_\omega Z_\omega \rangle$ that is used to transform the time-dependent Jacobian matrix of Eq. (39) into the time-independent Jacobian matrix (55). The remaining six eigenvalues obtained from the Jacobian matrix (55) correspond to the spectrum of the problem and are discussed in Sect. 4.

4 Results and discussion

In this section, the linear stability of the steady straight-line rolling motion, steady spinning around a vertical diameter and the circular steady motion are analysed in detail.

4.1 Linear stability of the steady straight-line rolling motion

First, the linear stability of the steady straight-line rolling motion of the toroidal wheel is studied. This motion corresponds to a limit case of the circular steady motion (22), with $\omega \to 0$, $\rho \to \infty$ and $\phi_0 \to 0$. This reference motion can be expressed as:

$$\begin{aligned} &x_C^0(t) = \Omega R t, && y_C^0(t) = 0, \\ &\psi^0(t) = 0, && \phi^0(t) = 0, \\ &\theta^0(t) = \Omega t. \end{aligned} \tag{56}$$

Note that Eq. (22), particularized for $\omega \to 0$ and $\rho \to \infty$, yield $x_C^0(t) \to 0$, $y_C^0(t) = \Omega R t$ and $\psi^0(t) = \dfrac{\pi}{2}$, which corresponds to the toroidal wheel moving along the Y_1-axis. For simplicity, the equivalent reference motion defined by Eq. (56), corresponding to the straight-line rolling of the wheel along the X_1-axis (see Fig. 5), is considered. In vector form, the reference motion of Eq. (56) is given by $\boldsymbol{x}^0(t) = \boldsymbol{\Omega}^0 t$, with $\boldsymbol{\Omega}^0 = \left(\Omega R \; 0 \; 0 \; 0 \; \Omega\right)^{\mathrm{T}}$. In the steady straight-line rolling motion, the values of the Lagrange multipliers, denoted as $\boldsymbol{\Lambda}_{\mathrm{S}}^0$, are given by:

$$\boldsymbol{\Lambda}_{\mathrm{S}}^0 = \left(\Lambda_{\mathrm{S},1}^0 \; \Lambda_{\mathrm{S},2}^0\right)^{\mathrm{T}} = \left(0 \; 0\right)^{\mathrm{T}}. \tag{57}$$

The Jacobian matrix of Eq. (55) can be particularized for the reference motion (56). The following system of linear equations, involving the yaw, lean and roll angles,

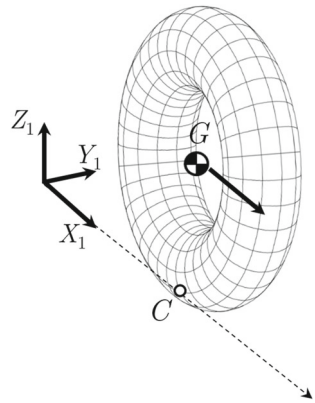

Fig. 5 Steady straight-line rolling motion of the toroidal wheel

is obtained:

$$\begin{aligned} \ddot{\tilde{\psi}} &= -2\mu_1^i(\eta)\,\Omega\dot{\tilde{\phi}}, \\ \ddot{\tilde{\phi}} &= \frac{2}{3}\mu_2^i(\eta)\,\frac{g}{R}\tilde{\phi} \\ &\quad + \frac{4}{3}\mu_3^i(\eta)\,\Omega\dot{\tilde{\psi}}, \\ \ddot{\tilde{\theta}} &= 0, \end{aligned} \tag{58}$$

where $\mu_j^i(\eta)$ are functions of the torus aspect ratio η, with $i = \{s, h\}$ and $j = 1 \ldots 3$, given by:

$$\begin{aligned} &\mu_1^s(\eta) = \frac{3\eta^2+4}{5\eta^2+4}, \quad \mu_1^h(\eta) = \frac{3\eta^2+2}{5\eta^2+2}, \\ &\mu_2^s(\eta) = \frac{12(1+\eta)}{13\eta^2+16\eta+12}, \quad \mu_2^h(\eta) = \frac{6(1+\eta)}{9\eta^2+8\eta+6}, \\ &\mu_3^s(\eta) = \frac{21\eta^2+24\eta+24}{26\eta^2+32\eta+24}, \quad \mu_3^h(\eta) = \frac{15\eta^2+12\eta+12}{18\eta^2+16\eta+12}. \end{aligned} \tag{59}$$

The linearized equations (58) are also valid for the steady straight-line motion of the rolling hoop, which corresponds to the limit case $\eta \to 0$. Note that $\mu_j^i(0) = 1$. As can be seen in Eq. (58), the equation associated with the forward motion, $\ddot{\tilde{\theta}} = 0$, is decoupled from the following two coupled linear system of differential equations, involving the yaw and lean angles of the wheel:

$$\begin{pmatrix} \ddot{\tilde{\psi}} \\ \ddot{\tilde{\phi}} \end{pmatrix} + \underbrace{\Omega \begin{pmatrix} 0 & c_{\mathrm{S}_1} \\ c_{\mathrm{S}_2} & 0 \end{pmatrix}}_{\boldsymbol{G}_{\mathrm{S}}} \begin{pmatrix} \dot{\tilde{\psi}} \\ \dot{\tilde{\phi}} \end{pmatrix}$$

$$+\underbrace{\begin{pmatrix} k_{S_1} & 0 \\ 0 & k_{S_2} \end{pmatrix}}_{\boldsymbol{K}_S} \begin{pmatrix} \tilde{\psi} \\ \tilde{\phi} \end{pmatrix} = \begin{pmatrix} 0 \\ 0 \end{pmatrix}, \tag{60}$$

with $c_{S_1} = 2\mu_1^i(\eta)$, $c_{S_2} = -\frac{4}{3}\mu_3^i(\eta)$, $k_{S_1} = 0$ and $k_{S_2} = -\frac{2}{3}\mu_2^i(\eta)\frac{g}{R}$. In Eq. (60), $\boldsymbol{K}_S$ and $\boldsymbol{G}_S$ are the stiffness and velocity-dependent matrices, respectively.

The following set of eigenvalues, associated with the linear system of equations (58), is obtained:

$$\boldsymbol{\lambda}_S = \left(\boldsymbol{0}_{1\times 4}\ \lambda_S^1\ \lambda_S^2\right)^T, \tag{61}$$

with $\lambda_S^1 = \varphi^i(\eta, \omega_0)\sqrt{\zeta^i\left(\eta, \bar{\Omega}\right)}$ and $\lambda_S^2 = -\varphi^i(\eta, \omega_0)\sqrt{\zeta^i\left(\eta, \bar{\Omega}\right)}$. The functions φ^i and ζ^i, with $i = \{s, h\}$, are given by:

$$\begin{aligned}
\varphi^s(\eta, f_0) &= \frac{2\omega_0}{\sqrt{\left(5\eta^2+4\right)\left(13\eta^2+16\eta+12\right)}}, \\
\zeta^s\left(\eta, \bar{\Omega}\right) &= \left(10\eta^2+8\right)(1+\eta) - \bar{\Omega}^2 \\
&\quad \times \left(21\eta^4+24\eta^3+52\eta^2+32\eta+32\right), \\
\varphi^h(\eta, f_0) &= \frac{2\omega_0}{\sqrt{\left(5\eta^2+2\right)\left(9\eta^2+8\eta+6\right)}}, \\
\zeta^h\left(\eta, \bar{\Omega}\right) &= \left(5\eta^2+2\right)(1+\eta) - \bar{\Omega}^2 \\
&\quad \times \left(15\eta^4+12\eta^3+22\eta^2+8\eta+8\right).
\end{aligned} \tag{62}$$

The eigenvalues of Eq. (61), particularized for the case of the rolling hoop ($\eta \to 0$), become:

$$\begin{aligned}
\boldsymbol{\lambda}_S^1\Big|_{\eta\to 0} &= \frac{\sqrt{6}}{3}\omega_0\sqrt{1-4\bar{\Omega}^2}, \\
\boldsymbol{\lambda}_S^2\Big|_{\eta\to 0} &= -\frac{\sqrt{6}}{3}\omega_0\sqrt{1-4\bar{\Omega}^2}.
\end{aligned} \tag{63}$$

In Eq. (61), two null and two nonzero eigenvalues are associated with the system of equations (60). Note that, since the stiffness matrix $\boldsymbol{K}_S$ of Eq. (60) is degenerate ($k_{S_1} = 0$), only two nonzero eigenvalues are obtained. Furthermore, the remaining two null eigenvalues in Eq. (61) correspond to the forward motion as a rigid body of the rolling wheel.

From the eigenvalues of Eq. (63), it can be seen that the gyroscopic stabilization of the rolling hoop is obtained for $\bar{\Omega}_c = \frac{1}{2}$. Therefore, the critical rotational speed Ω_c for which the stabilization is achieved is given by:

$$\bar{\Omega}_c = \frac{1}{2} \Rightarrow \Omega_c = \frac{1}{2}\sqrt{\frac{g}{R}}. \tag{64}$$

This result corresponds to the critical rolling speed of the rolling hoop found in the literature [31,33], validating the linear stability analysis.

In the case of a toroidal wheel of aspect ratio η, the value of $\bar{\Omega}$ for which the gyroscopic stabilization is obtained is denoted as $\bar{\Omega}_{\eta c}^i$, with $i = \{s, h\}$. From the non-null eigenvalues of Eq. (61), the boundary that determines the linear stability of the steady straight-line rolling motion is therefore given by $\zeta^i\left(\eta, \bar{\Omega}_{\eta c}^i\right) = 0$. The values of $\bar{\Omega}_{\eta c}^i$, for the solid and hollow cases, are given by:

$$\bar{\Omega}_{\eta c}^s = \sqrt{\frac{\left(10\eta^2+8\right)(1+\eta)}{21\eta^4+24\eta^3+52\eta^2+32\eta+32}}, \tag{65}$$

$$\bar{\Omega}_{\eta c}^h = \sqrt{\frac{\left(5\eta^2+2\right)(1+\eta)}{15\eta^4+12\eta^3+22\eta^2+8\eta+8}}. \tag{66}$$

From Eq. (64)–(66), the following relation is obtained:

$$\bar{\Omega}_{\eta c}^i = \sqrt{\chi_i(\eta)}\,\bar{\Omega}_c, \tag{67}$$

with the functions χ_i:

$$\chi_s(\eta) = \frac{4\left(10\eta^2+8\right)(1+\eta)}{21\eta^4+24\eta^3+52\eta^2+32\eta+32}, \tag{68}$$

$$\chi_h(\eta) = \frac{4\left(5\eta^2+2\right)(1+\eta)}{15\eta^4+12\eta^3+22\eta^2+8\eta+8}. \tag{69}$$

Note that these functions verify $\chi_s(0) = \chi_h(0) = 1$. The critical rotational speed of the toroidal wheel verifies $\bar{\Omega}_{\eta c}^i < \Omega_c\ \forall \eta \neq 0$, for both the solid and hollow scenarios, since $\chi_s(\eta)$ and $\chi_h(\eta)$ are monotonically decreasing functions. Therefore, in the toroidal wheel case, a lower rotational speed than in the rolling hoop scenario is required to achieve the stabilization. The evolution of these functions with the torus aspect ratio η is shown in Fig. 6.

Figure 6 allows a comparison of the linear stability of the steady straight-line rolling motion between the solid and hollow toroidal wheels. The intersection of $\chi_s(\eta)$ and $\chi_h(\eta)$ occurs for $\eta^* \approx 0.7115$. For $\eta < \eta^*$, the gyroscopic stabilization is achieved for a lower rotational speed in the solid case, while the hollow scenario

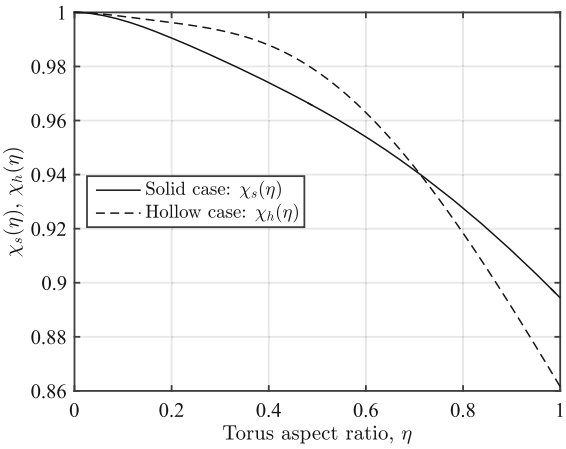

Fig. 6 Functions $\chi_s\,(\eta)$ and $\chi_h\,(\eta)$

becomes stable for a lower rotational speed than the solid case if $\eta > \eta^*$.

A comparison of the root loci of a solid toroidal wheel, with $\eta = 0.75$, and a hoop of equivalent radius is shown in Fig. 7a. The torus aspect ratio $\eta = 0.75$ has been chosen for a convenient visualization of the results. A numerical value of $\omega_0 = 1$ rad/s is considered. For $\Omega < \Omega^i_{\eta c}$, the rolling toroidal wheel presents a hyperbolic equilibrium, with two nonzero real eigenvalues of opposite sign, and is therefore unstable. In the case of $\Omega = \Omega^i_{\eta c}$, the eigenvalues coalesce and the wheel is still unstable. The gyroscopic stabilization is finally achieved for $\Omega > \Omega^i_{\eta c}$, presenting an elliptic equilibrium with a pair of purely imaginary eigenvalues. The cross markers in Fig. 7a correspond to $\Omega = 0$ rad/s, and the square markers to $\Omega = 1$ rad/s. Moreover, the unstable and stable regions are depicted in Fig. 7b. The transition from the unstable to the stable region is given by the critical rotational speed, which in the case of a solid toroidal wheel of $\eta = 0.75$ and $\omega_0 = 1$ rad/s, is $\Omega^s_{\eta c} = 0.4834$ rad/s.

Figure 8a, b show the evolution of the real and imaginary parts, respectively, of the eigenvalue λ^1_S with the rotational speed, for different torus aspect ratios: $\eta = \{0, 0.25, 0.5, 0.75, 1\}$. The results are analogous for the eigenvalue λ^2_S, with opposite sign. Note that, in line with Fig. 6, in which the functions $\chi_i\,(\eta)$ are shown,

Fig. 7 Eigenvalues of the rolling toroidal wheel in the steady straight-line rolling motion

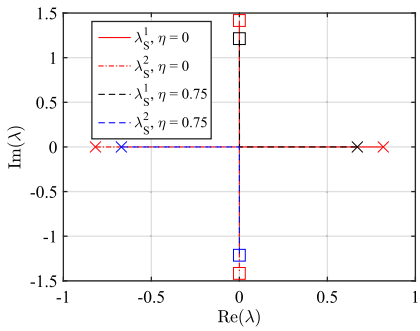

(a) Comparison of the root loci of the solid toroidal wheel ($\eta = 0.75$) and hoop ($\eta = 0$), with $\omega_0 = 1$ rad/s.

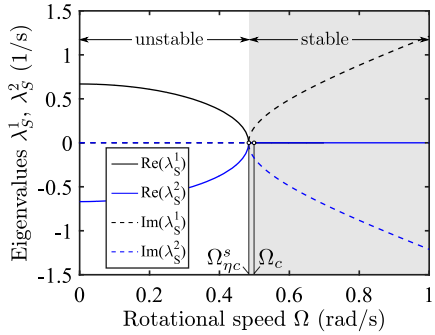

(b) Unstable and stable regions of the steady forward motion: evolution of the real and imaginary parts of the eigenvalues with the rotational speed Ω.

Fig. 8 Variation of the real and imaginary parts of λ^1_S (Re (λ^1_S) and Im (λ^1_S), respectively) with Ω, for $\eta = \{0, 0.25, 0.5, 0.75, 1\}$. The solid (S) and hollow (H) scenarios are shown

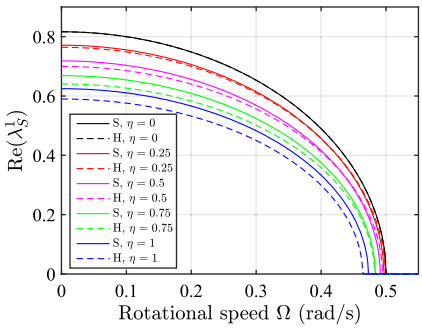

(a) Influence of η on Re (λ^1_S).

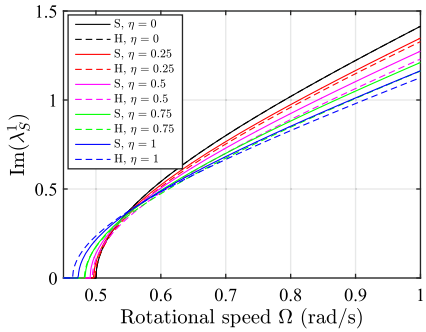

(b) Influence of η on Im (λ^1_S).

the rotational speed for which the real eigenvalue λ_S^1 becomes purely imaginary decreases as η increases, due to the stabilizing effect of the toroidal geometry. Figure 8a, b also allows a comparison betweeen the solid and hollow scenarios. For a torus aspect ratio lower than $\eta^* \approx 0.7115$ ($\eta = 0.25$ and $\eta = 0.5$ in Fig. 8a, b), the gyroscopic stabilization is achieved and the eigenvalue λ_S^1 turns purely imaginary for a lower rotational speed in the solid case, while the hollow scenario becomes stable for a lower rotational speed than the solid case if $\eta > \eta^*$ ($\eta = 0.75$ and $\eta = 1$ in Fig. 8a, b). This behavior is consistent with the evolution of the functions $\chi_s(\eta)$ and $\chi_h(\eta)$ in Fig. 6.

4.2 Linear stability of the steady spinning motion around a vertical diameter

The linear stability of the steady spinning motion around a vertical diameter is analysed. In this case, this reference motion corresponds to a limit case of the circular steady motion (22), with $\Omega \to 0$, $\rho \to 0$ and $\phi_0 \to 0$:

$$\begin{aligned} &x_C^0(t) = 0, && y_C^0(t) = 0, \\ &\psi^0(t) = \omega t, && \phi^0(t) = 0, \\ &\theta^0(t) = 0. \end{aligned} \tag{70}$$

In vector form, the reference motion of Eq. (70) can be expressed as $\boldsymbol{x}^0(t) = \boldsymbol{\omega}^0 t$, with $\boldsymbol{\omega}^0 = \begin{pmatrix} 0 & 0 & \omega & 0 & 0 \end{pmatrix}^{\mathrm{T}}$. In the steady spinning motion around a vertical diameter, the values of the Lagrange multipliers, denoted as $\boldsymbol{\Lambda}_\omega^0$, are given by:

$$\boldsymbol{\Lambda}_\omega^0 = \begin{pmatrix} \Lambda_{\omega,1}^0 & \Lambda_{\omega,2}^0 \end{pmatrix}^{\mathrm{T}} = \begin{pmatrix} 0 & 0 \end{pmatrix}^{\mathrm{T}}. \tag{71}$$

Figure 9 shows an arbitrary position of the toroidal wheel during the steady spinning motion.

Particularizing the Jacobian matrix (55) for this reference motion, the following system of linear equations of motion, involving the yaw, lean and roll angles, is obtained:

$$\begin{aligned} &\dddot{\tilde{\psi}} = 0, \\ &\dddot{\tilde{\phi}} = \left(\sigma_1^i(\eta)\,\omega^2 + \frac{2}{3}\sigma_2^i(\eta)\,\frac{g}{R} \right) \ddot{\tilde{\phi}} + \frac{4}{3}\sigma_3^i(\eta)\,\omega \dot{\tilde{\theta}}, \\ &\dddot{\tilde{\theta}} = -\frac{3}{2}\sigma_4^i(\eta)\,\omega \dot{\tilde{\phi}}, \end{aligned} \tag{72}$$

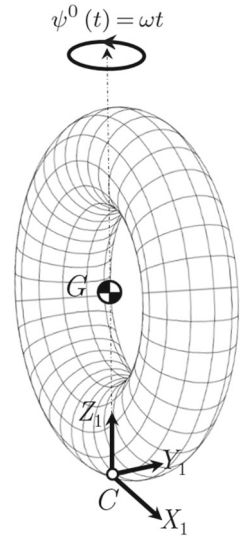

Fig. 9 Steady spinning motion around a vertical diameter of the toroidal wheel

where $\sigma_j^i(\eta)$ are the following functions of the torus aspect ratio, with $i = \{s, h\}$ and $j = 1 \ldots 4$:

$$\begin{aligned} \sigma_1^s(\eta) &= \frac{\eta^2 + 8\eta + 12}{13\eta^2 + 16\eta + 12}, & \sigma_1^h(\eta) &= \frac{\eta^2 + 4\eta + 6}{9\eta^2 + 8\eta + 6}, \\ \sigma_2^s(\eta) &= \frac{12(1+\eta)}{13\eta^2 + 16\eta + 12}, & \sigma_2^h(\eta) &= \frac{6(1+\eta)}{9\eta^2 + 8\eta + 6}, \\ \sigma_3^s(\eta) &= \frac{21\eta^2 + 24\eta + 24}{26\eta^2 + 32\eta + 24}, & \sigma_3^h(\eta) &= \frac{15\eta^2 + 12\eta + 12}{18\eta^2 + 16\eta + 12}, \\ \sigma_4^s(\eta) &= \frac{14\eta^2 + 24\eta + 24}{21\eta^2 + 24\eta + 24}, & \sigma_4^h(\eta) &= \frac{10\eta^2 + 12\eta + 12}{15\eta^2 + 12\eta + 12}. \end{aligned} \tag{73}$$

Note that $\sigma_j^i(0) = 1$. The linearized equations (72) are also valid for the rolling hoop ($\eta \to 0$). As can be seen in Eq. (72), the spinning motion is decoupled from the following two coupled linear system of differential equations, involving the lean and roll angles of the wheel:

$$\begin{pmatrix} \dddot{\tilde{\phi}} \\ \dddot{\tilde{\theta}} \end{pmatrix} + \underbrace{\omega \begin{pmatrix} 0 & c_{\omega_1} \\ c_{\omega_2} & 0 \end{pmatrix}}_{\boldsymbol{G}_\omega} \begin{pmatrix} \ddot{\tilde{\phi}} \\ \ddot{\tilde{\theta}} \end{pmatrix} + \underbrace{\begin{pmatrix} k_{\omega_1} & 0 \\ 0 & k_{\omega_2} \end{pmatrix}}_{\boldsymbol{K}_\omega} \begin{pmatrix} \dot{\tilde{\phi}} \\ \dot{\tilde{\theta}} \end{pmatrix} = \begin{pmatrix} 0 \\ 0 \end{pmatrix}, \tag{74}$$

with $c_{\omega_1} = -\frac{4}{3}\sigma_3^i(\eta)$, $c_{\omega_2} = \frac{3}{2}\sigma_4^i(\eta)$, $k_{\omega_1} = -\sigma_1^i(\eta)\,\omega^2 - \frac{2}{3}\sigma_2^i(\eta)\,\frac{g}{R}$ and $k_{\omega_2} = 0$. In Eq. (74),

$\boldsymbol{K}_\omega$ and $\boldsymbol{G}_\omega$ are the stiffness and velocity-dependent matrices of the steady spinning motion, respectively.

The following set of eigenvalues, associated with the linear system of equations (72), is obtained:

$$\boldsymbol{\lambda}_\omega = \left(\mathbf{0}_{1\times 4}\ \lambda_\omega^1\ \lambda_\omega^2\right)^{\mathrm{T}}, \tag{75}$$

with $\lambda_\omega^1 = \kappa^i\left(\eta, \omega_0\right)\sqrt{\varsigma^i\left(\eta, \bar{\omega}\right)}$ and $\lambda_\omega^2 = -\kappa^i\left(\eta,\ \omega_0\right)\sqrt{\varsigma^i\left(\eta, \bar{\omega}\right)}$. The functions κ^i and ς^i are given by:

$$\begin{aligned}
\kappa^s\left(\eta, \omega_0\right) &= \frac{\omega_0}{\sqrt{13\eta^2 + 16\eta + 12}},\\
\varsigma^s\left(\eta, \bar{\omega}\right) &= 8\left(1+\eta\right) - \bar{\omega}^2\left(13\eta^2 + 16\eta + 12\right),\\
\kappa^h\left(\eta, \omega_0\right) &= \frac{\omega_0}{\sqrt{9\eta^2 + 8\eta + 6}},\\
\varsigma^h\left(\eta, \bar{\omega}\right) &= 4\left(1+\eta\right) - \bar{\omega}^2\left(9\eta^2 + 8\eta + 6\right).
\end{aligned} \tag{76}$$

In the limit case of the rolling hoop, the eigenvalues of Eq. (75) become, for $\eta \to 0$:

$$\begin{aligned}
\boldsymbol{\lambda}_\omega^1\Big|_{\eta\to 0} &= \frac{\sqrt{6}}{3}\omega_0\sqrt{1 - \frac{3}{2}\bar{\omega}^2},\\
\boldsymbol{\lambda}_\omega^2\Big|_{\eta\to 0} &= -\frac{\sqrt{6}}{3}\omega_0\sqrt{1 - \frac{3}{2}\bar{\omega}^2}.
\end{aligned} \tag{77}$$

In Eq. (75), two null and two nonzero eigenvalues are associated with the system of equations (74). Note that, as in the steady straight-line rolling motion, the stiffness matrix $\boldsymbol{K}_\omega$ of Eq. (74) is degenerate ($k_{\omega_2} = 0$), and only two nonzero eigenvalues are obtained. Moreover, the remaining two null eigenvalues of Eq. (75) correspond to the spinning motion as a rigid body of the toroidal wheel, given by $\ddot{\tilde{\psi}} = 0$ in Eq. (72).

From the eigenvalues of Eq. (77), it can be seen that the gyroscopic stabilization of the hoop in the steady spinning motion occurs for $\bar{\omega}_c = \sqrt{\frac{2}{3}}$. Therefore, the critical spinning speed ω_c for which the stabilization of the hoop is achieved is given by:

$$\bar{\omega}_c = \sqrt{\frac{2}{3}} \Rightarrow \omega_c = \sqrt{\frac{2g}{3R}}. \tag{78}$$

This result corresponds to the critical spinning speed of the rolling hoop presented in [33], validating the linear stability analysis.

In a toroidal wheel of aspect ratio η, the boundary that determines the linear stability of the steady spinning motion around a vertical diameter is, by virtue of the non-null eigenvalues of Eq. (75), given by $\varsigma^i\left(\eta, \bar{\omega}_{\eta c}^i\right) = 0$, with $\bar{\omega}_{\eta c}^i$ being the value of $\bar{\omega}$ for which the gyroscopic stabilization of the spinning wheel occurs. The values of $\bar{\omega}_{\eta c}^i$, for the solid and hollow case, are given by:

$$\bar{\omega}_{\eta c}^s = \sqrt{\frac{8\left(1+\eta\right)}{13\eta^2 + 16\eta + 12}}, \tag{79}$$

$$\bar{\omega}_{\eta c}^h = \sqrt{\frac{4\left(1+\eta\right)}{9\eta^2 + 8\eta + 6}}. \tag{80}$$

From Eq. (78) and Eqs. (79)–(80), the following relation is obtained:

$$\bar{\omega}_{\eta c}^i = \sqrt{\gamma_i\left(\eta\right)}\,\bar{\omega}_c, \tag{81}$$

where the functions γ_i, with $i = \{s, h\}$, are given by:

$$\gamma_s\left(\eta\right) = \frac{12\left(1+\eta\right)}{13\eta^2 + 16\eta + 12}, \tag{82}$$

$$\gamma_h\left(\eta\right) = \frac{6\left(1+\eta\right)}{9\eta^2 + 8\eta + 6}. \tag{83}$$

Figure 10 shows the evolution of $\gamma_s\left(\eta\right)$ and $\gamma_h\left(\eta\right)$ with the torus aspect ratio. Both functions are monotonically decreasing, with $\gamma_s\left(0\right) = \gamma_h\left(0\right) = 1$. Therefore, as in the case of the steady straight-line rolling motion, the toroidal geometry results in a stabilizing effect with respect to the hoop, since the critical angular speed of the toroidal wheel verifies $\omega_{\eta c}^i < \omega_c\ \forall \eta \neq 0$, both in the solid and the hollow scenarios. Given that $\gamma_h < \gamma_s$

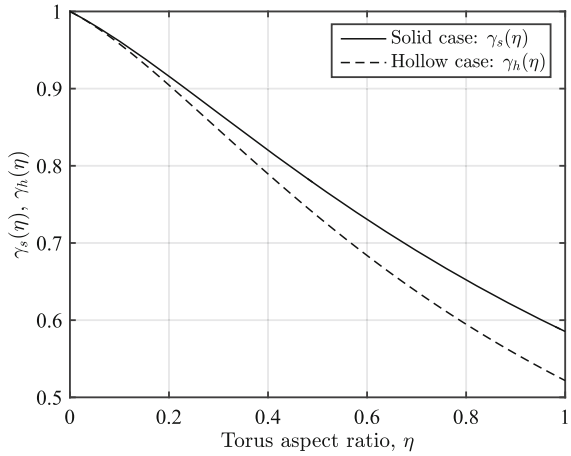

Fig. 10 Functions $\gamma_s\left(\eta\right)$ and $\gamma_h\left(\eta\right)$

$\forall \eta \neq 0$ (see Fig. 10), the gyroscopic stabilization is achieved for a lower angular speed in the hollow case.

Figure 11a shows a comparison of the root loci of a solid torus, with $\eta = 0.75$, and a hoop with equivalent radius. As in the case of Fig. 7, the torus aspect ratio $\eta = 0.75$ has been chosen for a convenient visualization of the results. A numerical value of $\omega_0 = 1$ rad/s is considered. In Fig. 11a, the cross marks correspond to $\omega = 0$ rad/s, and the square marks to $\omega = 1.5$ rad/s. Figure 11b represents the evolution of the real and complex parts of the eigenvalues λ_ω^1 and λ_ω^2 with the angular speed ω. The unstable and stable regions are also depicted in Fig. 11b. The transition from the unstable to the stable region is given by the critical angular speed, which in the case of a solid toroidal wheel with $\eta = 0.75$ and $\omega_0 = 1$ rad/s, is $\omega_{\eta c}^s \simeq 0.6687$ rad/s. The critical angular speed of the hoop with equivalent radius, $\omega_c = \sqrt{\frac{2}{3}} \simeq 0.8165$ rad/s, is also highlighted. The toroidal wheel, in the steady spinning motion around a vertical diameter, presents the same behaviour as in the steady straight-line rolling motion.

A hyperbolic equilibrium exists for $\omega < \omega_{\eta c}^i$, with two nonzero real eigenvalues of opposite sign, being unstable. For $\omega = \omega_{\eta i}^*$, the eigenvalues coalesce, with $\lambda_\omega^1 = \lambda_\omega^2 = 0$, and the system remains unstable. Lastly, when $\omega > \omega_{\eta c}^i$, the gyroscopic stabilization is achieved and the real eigenvalues turn into a complex conjugate pair, leading to an elliptic equilibrium.

The influence of the aspect ratio η on the real and imaginary parts of the eigenvalue λ_ω^1 is shown in Fig. 12. Figure 12a represents the variation of the real part $\mathrm{Re}\left(\lambda_\omega^1\right)$ with the angular speed ω, for a set of values of $\eta = \{0, 0.25, 0.5, 0.75, 1\}$. Similarly, Fig. 12b shows the imaginary part $\mathrm{Im}\left(\lambda_\omega^1\right)$. Note that, in consistency with the functions $\gamma_s(\eta)$ and $\gamma_h(\eta)$ of Eqs. (82) and (83), depicted in Fig. 10, the toroidal geometry leads to a stabilizing effect, since the value of ω for which the real eigenvalues become purely imaginary decreases as η increases. For a given torus aspect ratio η, the gyroscopic stabilization of the steady spinning motion around a vertical diameter is always achieved for a lower speed in the hollow scenario.

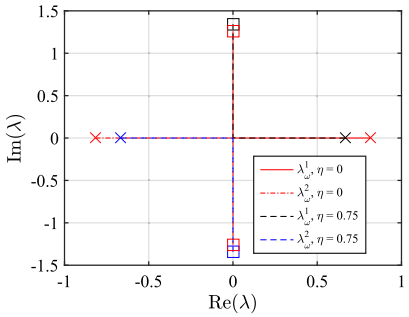

(a) Comparison of the root loci of the rolling toroidal wheel ($\eta = 0.75$) and hoop ($\eta = 0$), with $\omega_0 = 1$ rad/s.

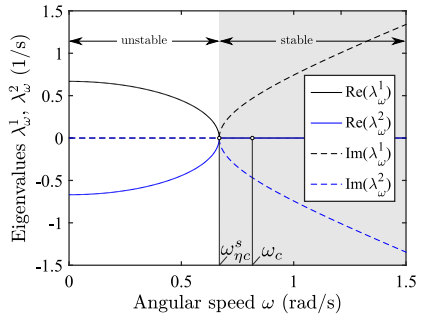

(b) Unstable and stable regions of the steady spinning motion around a vertical diameter: evolution of the real and imaginary parts of the eigenvalues with the angular speed ω.

Fig. 11 Eigenvalues of the rolling toroidal wheel in the steady spinning motion around a vertical diameter

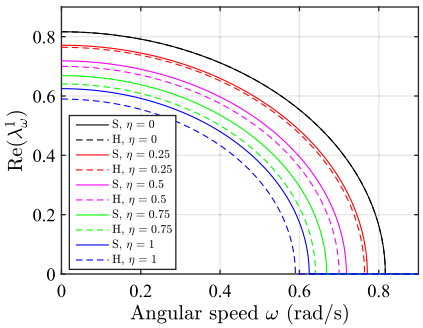

(a) Influence of η on $\mathrm{Re}\left(\lambda_\omega^1\right)$.

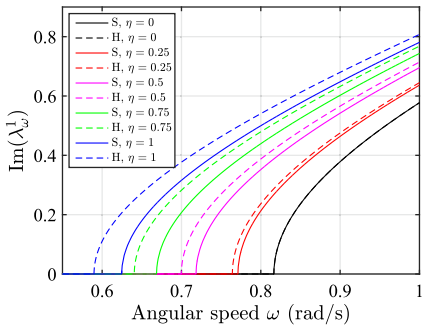

(b) Influence of η on $\mathrm{Im}\left(\lambda_\omega^1\right)$.

Fig. 12 Variation of the real and imaginary parts of λ_ω^1 ($\mathrm{Re}\left(\lambda_\omega^1\right)$ and $\mathrm{Im}\left(\lambda_\omega^1\right)$, respectively) with ω, for $\eta = \{0, 0.25, 0.5, 0.75, 1\}$. The solid (S) and hollow (H) scenarios are shown

4.3 Linear stability of the circular steady motion

The linear stability of the circular steady motion, which was defined in Eqs. (21) and (22), is analysed. From the Jacobian matrix of Eq. (55), the following system of linear equations, involving the yaw, lean and roll angles, is obtained:

$$\ddot{\tilde{\psi}} = \left(\delta_1^i(\eta,\phi_0)\,\omega + \delta_2^i(\eta,\phi_0)\,\Omega\right)\dot{\tilde{\phi}}, \tag{84}$$

$$\ddot{\tilde{\phi}} = \left(\delta_3^i(\eta,\phi_0)\,\omega^2 + \delta_4^i(\eta,\phi_0)\,\frac{g}{R} + \delta_5^i(\eta,\phi_0)\,\Omega\omega\right)\tilde{\phi} + \left(\delta_6^i(\eta,\phi_0)\,\omega + \delta_7^i(\eta,\phi_0)\,\Omega\right)\dot{\tilde{\psi}} + \delta_7^i(\eta,\phi_0)\,\omega\dot{\tilde{\theta}}, \tag{85}$$

$$\ddot{\tilde{\theta}} = \left(\delta_8^i(\eta,\phi_0)\,\omega + \delta_9^i(\eta,\phi_0)\,\Omega\right)\dot{\tilde{\phi}}, \tag{86}$$

where the functions $\delta_k^i(\eta,\phi_0)$, with $i = \{s,h\}$ and $k = 1\ldots9$, were introduced after Eq. (40) and their expressions can be found in "Appendix A". The linear system of equations (84)–(86), particularized for the case of the rolling hoop ($\eta \to 0$), becomes:

$$\ddot{\tilde{\psi}} = -\frac{2\Omega}{\cos(\phi_0)}\dot{\tilde{\phi}}, \tag{87}$$

$$\ddot{\tilde{\phi}} = \left(\omega^2\cos(2\phi_0) + \frac{2}{3}\frac{g}{R}\cos(\phi_0) - \frac{4}{3}\Omega\omega\sin(2\phi_0)\right)\tilde{\phi} + \left(\frac{4}{3}\Omega\cos(\phi_0) + \omega\sin(2\phi_0)\right)\dot{\tilde{\psi}} + \frac{4}{3}\omega\cos(\phi_0)\,\dot{\tilde{\theta}}, \tag{88}$$

$$\ddot{\tilde{\theta}} = \left(2\Omega\tan(\phi_0) - \frac{3}{2}\omega\cos(\phi_0)\right)\dot{\tilde{\phi}}. \tag{89}$$

Equations (84)–(86) can be rewritten as follows:

$$\begin{pmatrix} \ddot{\tilde{\psi}} \\ \ddot{\tilde{\phi}} \\ \ddot{\tilde{\theta}} \end{pmatrix} + \left(\underbrace{\omega \begin{pmatrix} 0 & c_{\omega_1} & 0 \\ c_{\omega_2} & 0 & c_{\omega_3} \\ 0 & c_{\omega_4} & 0 \end{pmatrix}}_{\boldsymbol{G}_c^{\omega}} + \underbrace{\Omega \begin{pmatrix} 0 & c_{\Omega_1} & 0 \\ c_{\Omega_2} & 0 & 0 \\ 0 & c_{\Omega_3} & 0 \end{pmatrix}}_{\boldsymbol{G}_c^{\Omega}} \right) \begin{pmatrix} \dot{\tilde{\psi}} \\ \dot{\tilde{\phi}} \\ \dot{\tilde{\theta}} \end{pmatrix} + \underbrace{\begin{pmatrix} 0 & 0 & 0 \\ 0 & k_{c_1} & 0 \\ 0 & 0 & 0 \end{pmatrix}}_{\boldsymbol{K}_c} \begin{pmatrix} \tilde{\psi} \\ \tilde{\phi} \\ \tilde{\theta} \end{pmatrix} = \begin{pmatrix} 0 \\ 0 \\ 0 \end{pmatrix}, \tag{90}$$

where $\boldsymbol{K}_c$ is the stiffness matrix, and $\boldsymbol{G}_c^{\omega}$, $\boldsymbol{G}_c^{\Omega}$ are velocity-dependent matrices, proportional to the angular and rotational speeds ω and Ω, respectively. In Eq. (84), $c_{\omega_1} = -\delta_1^i(\eta,\phi_0)$, $c_{\omega_2} = -\delta_6^i(\eta,\phi_0)$, $c_{\omega_3} = -\delta_7^i(\eta,\phi_0)$, $c_{\omega_4} = -\delta_8^i(\eta,\phi_0)$, $c_{\Omega_1} = -\delta_2^i(\eta,\phi_0)$, $c_{\Omega_2} = -\delta_7^i(\eta,\phi_0)$, $c_{\Omega_3} = -\delta_9^i(\eta,\phi_0)$ and $k_{c_1} = -\left(\delta_3^i(\eta,\phi_0)\,\omega^2 + \delta_4^i(\eta,\phi_0)\,\frac{g}{R} + \delta_5^i(\eta,\phi_0)\,\Omega\omega\right)$. In contrast to the linearized equations of motion associated with the steady straight-line rolling and spinning around a vertical diameter, given by Eqs. (58) and (72), respectively, equations (90) constitute a linear system of three coupled equations.

The following set of eigenvalues, associated with the linear system (90), is obtained:

$$\boldsymbol{\lambda}_c = \left(\boldsymbol{0}_{1\times4}\ \lambda_c^1\ \lambda_c^2\right)^{\mathrm{T}}, \tag{91}$$

where

$$\lambda_c^1 = \frac{\omega_0}{\sqrt{\beta_5^i(\eta,\phi_0)}}\sqrt{\mathcal{S}_\beta^i\left(\bar{\Omega},\bar{\omega},\phi_0,\eta\right)},$$
$$\lambda_c^2 = -\frac{\omega_0}{\sqrt{\beta_5^i(\eta,\phi_0)}}\sqrt{\mathcal{S}_\beta^i\left(\bar{\Omega},\bar{\omega},\phi_0,\eta\right)}, \tag{92}$$

and $\mathcal{S}_\beta^i$, with $i = \{s,h\}$, is given by:

$$\mathcal{S}_\beta^i\left(\bar{\Omega},\bar{\omega},\phi_0,\eta\right) = \beta_1^i(\eta,\phi_0) + \beta_2^i(\eta,\phi_0)\,\bar{\Omega}^2 + \beta_3^i(\eta,\phi_0)\,\bar{\Omega}\bar{\omega} + \beta_4^i(\eta,\phi_0)\,\bar{\omega}^2. \tag{93}$$

The analytical expressions of the functions β_k^i in Eqs. (92) and (93), with $i = \{s,h\}$ and $k = 1\ldots5$, can be found in "Appendix A".

The nonzero eigenvalues of the circular steady motion, presented in Eq. (92), become, for $\bar{\omega} \to 0$ and $\phi_0 \to 0$, those of the steady straight-line rolling motion of Eq. (61). Furthermore, in the limit case $\bar{\Omega} \to 0$ and $\phi_0 \to 0$, the eigenvalues (75) of the steady spinning motion around a vertical diameter are obtained. Therefore, the same eigenvalues of the linear stability analysis of the limit motions are obtained, validating the linear stability results of the circular steady motion. In the limit case of the rolling hoop, the eigenvalues of Eq. (92) become, for $\eta \to 0$:

$$\lambda_c^1\Big|_{\eta\to 0} = \frac{\sqrt{6}\omega_0}{3}\sqrt{\cos(\phi_0) - \frac{3}{2}\bar{\omega}^2 - 4\bar{\Omega}\left(\bar{\Omega} + \bar{\omega}\sin(\phi_0)\right)},$$
$$\lambda_c^2\Big|_{\eta\to 0} = -\frac{\sqrt{6}\omega_0}{3}\sqrt{\cos(\phi_0) - \frac{3}{2}\bar{\omega}^2 - 4\bar{\Omega}\left(\bar{\Omega} + \bar{\omega}\sin(\phi_0)\right)}. \tag{94}$$

The equilibrium equations (27) and (28), particularized for a given aspect ratio η, can be represented as the following surface:

$$S_e^i\left(\bar{\Omega}, \bar{\omega}, \phi_0\right) = 0, \text{ with } i = \{s, h\}. \tag{95}$$

Moreover, the function $\mathcal{S}_\beta^i\left(\bar{\Omega}, \bar{\omega}, \phi_0, \eta\right)$, particularized for a torus aspect ratio η, is denoted as $S_\beta^i\left(\bar{\Omega}, \bar{\omega}, \phi_0\right)$. Therefore, the boundary that determines the linear stability of the circular steady motion of a toroidal wheel with aspect ratio η is given by the intersection of the equilibrium surface $S_e^i\left(\bar{\Omega}, \bar{\omega}, \phi_0\right) = 0$ of Eq. (95) and the surface $S_\beta^i\left(\bar{\Omega}, \bar{\omega}, \phi_0\right) = 0$:

$$\begin{cases} S_e^i\left(\bar{\Omega}, \bar{\omega}, \phi_0\right) = 0, \\ S_\beta^i\left(\bar{\Omega}, \bar{\omega}, \phi_0\right) = 0. \end{cases} \tag{96}$$

Figure 13 shows a three-dimensional view of the stability boundaries, obtained for different aspect ratios η. In particular, the numerical values of $\eta = \{0, 0.25, 0.5, 0.75, 1\}$ are considered. Note that, for convenience, the absolute value of the equilibrium lean angle $|\phi_0|$ is used. To verify the results, the same curve is obtained, for $\eta = 0$, in the solid and hollow scenarios (see Fig. 13), and tallies with the result obtained for the rolling hoop.

Moreover, Fig. 14 shows the projections of the stability boundaries on the $\bar{\omega}$–$\bar{\Omega}$ plane. The stability results obtained in the study of the limit motions (steady straight-line rolling in Sect. 4.1 and spinning around a vertical diameter in Sect. 4.2) can also be observed in

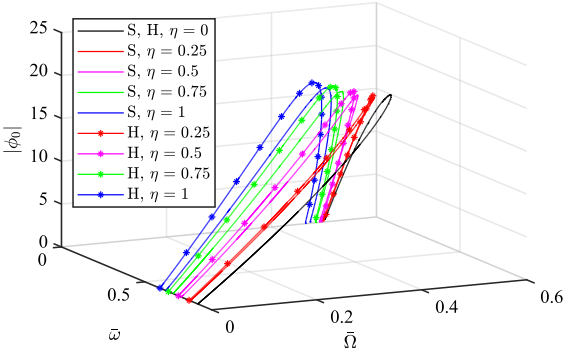

Fig. 13 Stability boundaries of the circular steady motion. The solid (S) and hollow (H) cases, for $\eta = \{0, 0.25, 0.5, 0.75, 1\}$, are shown

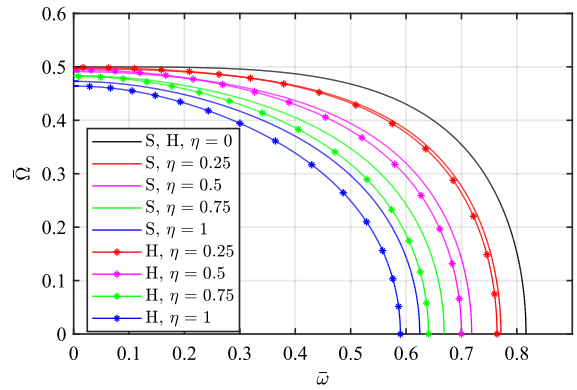

Fig. 14 Projections of the stability boundaries, in the solid (S) and hollow (H) case, for $\eta = \{0, 0.25, 0.5, 0.75, 1\}$

Fig. 14. For $\bar{\omega} \to 0$, the intersections of the projections with the $\bar{\Omega}$-axis of Fig. 14 correspond to $\bar{\Omega}_{\eta c}^i$, and are in accordance with the expression of $\bar{\Omega}_{\eta c}^i$ in Eq. (67) and the functions χ_s and χ_h of Eqs. (68) and (69), respectively. Likewise, for $\bar{\Omega} \to 0$, the intersections of the projections with the $\bar{\omega}$-axis correspond to $\bar{\omega}_{\eta c}^i$, and are in accordance with the expression of $\bar{\omega}_{\eta c}^i$ in Eq. (81) and the functions γ_s and γ_h of Eqs. (82) and (83), respectively. Note that the torus aspect ratio η of the toroidal wheel greatly impacts on the stability boundaries. As η increases, the stability is achieved for a lower combination of rotational speed $\bar{\Omega}$ and angular speed $\bar{\omega}$.

Lastly, Fig. 15 shows, for a solid toroidal wheel, the stability boundaries on the equilibrium surfaces $S_e^s\left(\bar{\Omega}, \bar{\omega}, \phi_0\right) = 0$, for $\eta = 0$ and $\eta = 0.75$. The torus aspect ratio $\eta = 0.75$ has been chosen for a convenient visualization of the results. The part of the equi-

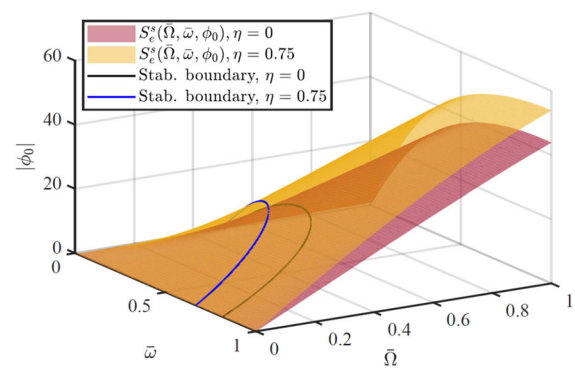

Fig. 15 Stability boundaries, for $\eta = 0$ and $\eta = 0.75$, on the equilibrium surfaces $S_e^s\left(\bar{\Omega}, \bar{\omega}, \phi_0\right) = 0$

librium surface below the stability boundary represents the unstable region, and the toroidal wheel presents a hyperbolic equilibrium, where the nonzero eigenvalues λ_c^1 and λ_c^2 of Eq. (92) are real with opposite sign. On the stability boundary, the eigenvalues λ_c^1 and λ_c^2 coalesce and become null. Finally, the part of the equilibrium surface above the stability boundary is the stable region, corresponding to an elliptic equilibrium, where the eigenvalues λ_c^1 and λ_c^2 are purely imaginary.

In the particular case of a circular trajectory with large radius compared to the radius of the wheel ($\rho \gg R$), an accurate expression of the rotational speed required for stability in the circular steady motion can be analytically found. Paris et al. [31] showed this result for the rolling disk and hoop. Particularizing the eigenvalues (94) for the condition $\rho \gg R$, which by virtue of Eq. (24) is equivalent to $\bar{\omega} \ll \bar{\Omega}$, the critical rotational speed $\bar{\Omega}_c^*$ is obtained:

$$\bar{\Omega}_c^* = \frac{1}{2}\sqrt{\cos(\phi_0)} = \bar{\Omega}_c\sqrt{\cos(\phi_0)}, \tag{97}$$

where $\bar{\Omega}_c$ is the critical rotational speed of the rolling hoop in the steady straight-line rolling motion, defined in Eq. (64). Equation (97) provides the same result shown by Paris et al. [31]. From Eq. (97), it can be seen that the critical rolling speed for stability in the circular steady motion $\bar{\Omega}_c^*$ (corresponding to $\bar{\omega} \ll \bar{\Omega}$) is lower than in the steady straight-line rolling motion $\bar{\Omega}_c$ (associated with $\bar{\omega} = 0$). Similarly, in the case of a toroidal wheel describing a circular trajectory with large radius compared to the radius of the wheel, the expression of the critical rolling speed required for stability can be obtained:

$$\bar{\Omega}_{\eta c}^{i*} = \sqrt{-\frac{\beta_1^i(\eta, \phi_0)}{\beta_2^i(\eta, \phi_0)}}, \tag{98}$$

where the functions $\beta_1^i(\eta, \phi_0)$ and $\beta_2^i(\eta, \phi_0)$ can be found in "Appendix A". The functions $\beta_1^i(\eta, \phi_0)$ and $\beta_2^i(\eta, \phi_0)$ have opposite signs. As in the case of the rolling hoop, and as can be seen in the projections of the stability boundaries shown in Fig. 14, the critical rolling speed in the circular steady motion $\bar{\Omega}_{\eta c}^{i*}$ (corresponding to $\bar{\omega} \ll \bar{\Omega}$) is lower than the critical rolling speed in the steady straight-line rolling $\bar{\Omega}_{\eta c}^i$ (associated with $\bar{\omega} = 0$).

5 Conclusions

In this paper, the linear stability of the rolling toroidal wheel was analysed in detail. The nonlinear equations of motion of the solid and hollow toroidal wheel with circular-cross section were derived. The circular steady motion, which constitutes a relative equilibrium of the system, was obtained. The linearized equations of motion along this reference solution were analytically derived as a function of the torus aspect ratio η.

First, the linear stability of the steady straight-line rolling motion and the steady spinning motion around a vertical diameter, which correspond to limit motions of the circular steady solution, were studied. In the steady straight-line rolling motion, the corresponding eigenvalues and the critical rolling speed required for stabilization $\Omega_{\eta c}^i$ were analytically obtained. For $\Omega < \Omega_{\eta c}^i$, the rolling toroidal wheel presents a hyperbolic equilibrium, with two nonzero real eigenvalues of opposite sign, and is therefore unstable. In the case of $\Omega = \Omega_{\eta c}^i$, the eigenvalues coalesce and the wheel is still unstable. Finally, for $\Omega > \Omega_{\eta c}^i$, an elliptic equilibrium with a pair of purely imaginary eigenvalues is obtained, becoming stable. A comparison between the solid and hollow scenarios was also performed. Below a critical torus aspect ratio η^*, the gyroscopic stabilization is achieved for a lower rolling speed in the solid case, while for $\eta > \eta^*$, the hollow toroidal wheel becomes stable for a lower rotational speed than the solid case. Similarly, the eigenvalues and the critical spinning speed $\omega_{\eta c}^i$ of the steady spinning motion around a vertical diameter were derived. For $\omega < \omega_{\eta c}^i$, a hyperbolic equilibrium is obtained, with two nonzero real eigenvalues of opposite sign, being unstable. For $\omega = \omega_{\eta c}^i$, the eigenvalues coalesce and, for $\omega > \omega_{\eta c}^i$, the stability is achieved, obtaining an elliptic equilibrium with a pair of purely imaginary eigenvalues. In this reference motion, the stability is always achieved for a lower spinning speed in the hollow toroidal wheel. For both limit motions, the eigenvalues and the critical rolling and spinning speeds were particularized for $\eta = 0$, obtaining the same results of the rolling hoop. A comparison between the toroidal wheel and the rolling hoop was also included, showing the stabilizing effect of the toroidal geometry.

Concerning the linear stability of the circular steady motion, the corresponding eigenvalues were analytically obtained, for both the solid and hollow scenarios. The influence of the torus aspect ratio η on the stabil-

ity boundary was studied, and it was shown that, as η increases, a lower combination of rolling speed Ω and spinning speed ω was required to achieve the stability. The equilibrium surfaces, with the corresponding stability boundaries, were shown for $\eta = 0.75$ and the hoop case ($\eta = 0$). The stability results of the steady straight-line rolling motion and the steady spinning motion around a vertical diameter were analytically validated by particularizing the eigenvalues of the circular steady motion for these reference solutions. Moreover, these results were also verified with the projections of the stability boundaries on the $\bar{\omega} - \bar{\Omega}$ plane. Lastly, in the case of a circular trajectory with large radius compared to the radius of the wheel ($\rho \gg R$), an accurate expression of the critical rolling speed required for the stability of the circular steady motion was obtained.

It is important to note that, in this work, all the results have been obtained for a toroidal wheel with a circular-cross section. In future work, the influence of different geometries of the cross-section on the stability of the relative equilibria could be studied. Moreover, the bifurcations of the system could be analysed and compared with those of the rolling hoop and disk.

Acknowledgements The authors have not disclosed any acknowledgement.

Funding Funding for open access publishing: Universidad de Sevilla/CBUA This work was supported by Grant FPU18/05598 of the Spanish Ministry of Science, Innovation and Universities and project US-1380740 of Consejería de Universidad, Investigación e Innovación, Junta de Andalucía.

Data availability The datasets generated during and/or analysed during the current study are available from the corresponding author on reasonable request.

Declarations

Conflict of interest The authors declare that they have no conflict of interest.

A Appendix

The functions $\delta_k^i(\eta,\phi_0)$, with $i = \{s,h\}$ and $k = 1\ldots 9$, are given by:

$$\delta_1^s(\eta,\phi_0) = -\frac{2\eta^4\sin(3\phi_0) - 34\eta^4\sin(\phi_0) - 28\eta^3\sin(2\phi_0) - 56\eta^2\sin(\phi_0) + 8\eta^2\sin(3\phi_0) - 16\eta\sin(2\phi_0)}{\cos(\phi_0)\left(39\eta^4 - 4\eta^4\cos^2(\phi_0) + 40\eta^3\cos(\phi_0) + 84\eta^2 - 16\eta^2\cos^2(\phi_0) + 32\eta\cos(\phi_0) + 32\right)},$$

$$\delta_2^s(\eta,\phi_0) = -\frac{42\eta^4 + 48\eta^3\cos(\phi_0) + 104\eta^2 + 64\eta\cos(\phi_0) + 64}{\cos(\phi_0)\left(39\eta^4 - 4\eta^4\cos^2(\phi_0) + 40\eta^3\cos(\phi_0) + 84\eta^2 - 16\eta^2\cos^2(\phi_0) + 32\eta\cos(\phi_0) + 32\right)},$$

$$\delta_3^s(\eta,\phi_0) = \frac{\eta^2\cos(2\phi_0) + 8\eta\cos(\phi_0) + 12\cos(2\phi_0)}{13\eta^2 + 16\eta\cos(\phi_0) + 12}, \quad \delta_4^s(\eta,\phi_0) = \frac{8\cos(\phi_0)}{\left(13\eta^2 + 16\eta\cos(\phi_0) + 12\right)(1+\eta)},$$

$$\delta_5^s(\eta,\phi_0) = -\frac{14\eta^2\sin(\phi_0) + 8\eta\sin(2\phi_0) + 16\sin(\phi_0)}{13\eta^2 + 16\eta\cos(\phi_0) + 12}, \quad \delta_6^s(\eta,\phi_0) = \frac{\eta^2\sin(2\phi_0) + 16\eta\sin(\phi_0) + 12\sin(2\phi_0)}{13\eta^2 + 16\eta\cos(\phi_0) + 12},$$

$$\delta_7^s(\eta,\phi_0) = \frac{14\eta^2\cos(\phi_0) + 8\eta + 8\eta\cos^2(\phi_0) + 16\cos(\phi_0)}{13\eta^2 + 16\eta\cos(\phi_0) + 12},$$

$$\delta_8^s(\eta,\phi_0) = \frac{\eta^4\cos^2(\phi_0) - 36\eta^4 - 60\eta^3\cos(\phi_0) - 64\eta^2 - 24\eta^2\cos^2(\phi_0) - 48\eta\cos(\phi_0) - 48\cos^2(\phi_0)}{\cos(\phi_0)\left(39\eta^4 - 4\eta^4\cos^2(\phi_0) + 40\eta^3\cos(\phi_0) + 84\eta^2 - 16\eta^2\cos^2(\phi_0) + 32\eta\cos(\phi_0) + 32\right)},$$

$$\delta_9^s(\eta,\phi_0) = \frac{38\eta^4\sin(\phi_0) + 4\eta^4\sin^3(\phi_0) + 22\eta^3\sin(2\phi_0) + 88\eta^2\sin(\phi_0) + 16\eta^2\sin^3(\phi_0) + 24\eta\sin(2\phi_0) + 64\sin(\phi_0)}{\cos(\phi_0)\left(39\eta^4 - 4\eta^4\cos^2(\phi_0) + 40\eta^3\cos(\phi_0) + 84\eta^2 - 16\eta^2\cos^2(\phi_0) + 32\eta\cos(\phi_0) + 32\right)},$$

$$\delta_1^h(\eta,\phi_0) = -\frac{\eta^4\sin(3\phi_0) - 23\eta^4\sin(\phi_0) - 14\eta^3\sin(2\phi_0) - 22\eta^2\sin(\phi_0) + 2\eta^2\sin(3\phi_0) - 4\eta\sin(2\phi_0)}{\cos(\phi_0)\left(27\eta^4 - 2\eta^4\cos^2(\phi_0) + 20\eta^3\cos(\phi_0) + 34\eta^2 - 4\eta^2\cos^2(\phi_0) + 8\eta\cos(\phi_0) + 8\right)},$$

$$\delta_2^h(\eta,\phi_0) = -\frac{30\eta^4 + 24\eta^3\cos(\phi_0) + 44\eta^2 + 16\eta\cos(\phi_0) + 16}{\cos(\phi_0)\left(27\eta^4 - 2\eta^4\cos^2(\phi_0) + 20\eta^3\cos(\phi_0) + 34\eta^2 - 4\eta^2\cos^2(\phi_0) + 8\eta\cos(\phi_0) + 8\right)},$$

$$\delta_3^h(\eta,\phi_0)=\frac{\eta^2\cos(2\phi_0)+4\eta\cos(\phi_0)+6\cos(2\phi_0)}{9\eta^2+8\eta\cos(\phi_0)+6},\ \delta_4^h(\eta,\phi_0)=\frac{4\cos(\phi_0)}{\left(9\eta^2+8\eta\cos(\phi_0)+6\right)(1+\eta)},$$
$$\delta_5^h(\eta,\phi_0)=-\frac{10\eta^2\sin(\phi_0)+4\eta\sin(2\phi_0)+8\sin(\phi_0)}{9\eta^2+8\eta\cos(\phi_0)+6},\ \delta_6^h(\eta,\phi_0)=\frac{\eta^2\sin(2\phi_0)+8\eta\sin(\phi_0)+6\sin(2\phi_0)}{9\eta^2+8\eta\cos(\phi_0)+6},$$
$$\delta_7^h(\eta,\phi_0)=\frac{10\eta^2\cos(\phi_0)+4\eta+4\eta\cos^2(\phi_0)+8\cos(\phi_0)}{9\eta^2+8\eta\cos(\phi_0)+6},$$
$$\delta_8^h(\eta,\phi_0)=-\frac{\eta^4\cos^2(\phi_0)+24\eta^4+30\eta^3\cos(\phi_0)+24\eta^2+16\eta^2\cos^2(\phi_0)+12\eta\cos(\phi_0)+12\cos^2(\phi_0)}{\cos(\phi_0)\left(27\eta^4-2\eta^4\cos^2(\phi_0)+20\eta^3\cos(\phi_0)+34\eta^2-4\eta^2\cos^2(\phi_0)+8\eta\cos(\phi_0)+8\right)},$$
$$\delta_9^h(\eta,\phi_0)=\frac{28\eta^4\sin(\phi_0)+2\eta^4\sin^3(\phi_0)+11\eta^3\sin(2\phi_0)+40\eta^2\sin(\phi_0)+4\eta^2\sin^3(\phi_0)+6\eta\sin(2\phi_0)+16\sin(\phi_0)}{\cos(\phi_0)\left(27\eta^4-2\eta^4\cos^2(\phi_0)+20\eta^3\cos(\phi_0)+34\eta^2-4\eta^2\cos^2(\phi_0)+8\eta\cos(\phi_0)+8\right)}. \tag{99}$$

The functions β_k^i, with $i=\{s,h\}$ and $k=1\ldots5$, are:

$$\begin{aligned}
\beta_1^s(\eta,\phi_0)&=8(1+\eta)\left(\left(39\eta^4+84\eta^2+32\right)\cos^2(\phi_0)\right.\\
&\left.+\left(40\eta^3+32\eta\right)\cos^3(\phi_0)-\left(4\eta^4+16\eta^2\right)\cos^4(\phi_0)\right),\\
\beta_2^s(\eta,\phi_0)&=-4\left(84\eta^5+208\eta^3+128\eta\right.\\
&+\left(147\eta^6+628\eta^4+768\eta^2+256\right)\cos(\phi_0)\\
&+\left(252\eta^5+624\eta^3+384\eta\right)\cos^2(\phi_0)\\
&\left.+\left(96\eta^4+128\eta^2\right)\cos^3(\phi_0)\right),\\
\beta_3^s(\eta,\phi_0)&=\frac{1}{1+\eta\cos(\phi_0)}\\
&\left(\left(462\eta^7+1216\eta^5-1568\eta^3-2304\eta\right)\sin(\phi_0)\right.\\
&+\left(207\eta^6+148\eta^4-864\eta^2-512\right)\sin(2\phi_0)\\
&-\left(462\eta^7+1264\eta^5-1248\eta^3-1792\eta\right)\sin^3(\phi_0)\\
&+\left(536\eta^6-448\eta^4-1152\eta^2\right)\sin(\phi_0)\cos^3(\phi_0)\\
&-\left(112\eta^7+448\eta^5+512\eta^3\right)\sin(\phi_0)\cos^4(\phi_0)\\
&\left.-\left(32\eta^6+128\eta^4\right)\sin(\phi_0)\cos^5(\phi_0)\right),\\
\beta_4^s(\eta,\phi_0)&=\frac{1}{(1+\eta\cos(\phi_0))^2}\left(288\eta^5+512\eta^3\right.\\
&+\left(105\eta^6+408\eta^4-400\eta^2-384\right)\cos(\phi_0)\\
&-\left(654\eta^7+2160\eta^5+3104\eta^3+1280\eta\right)\cos^2(\phi_0)\\
&-\left(471\eta^8+3488\eta^6+6464\eta^4+3136\eta^2\right)\cos^3(\phi_0)\\
&-\left(1424\eta^7+5144\eta^5+4160\eta^3+384\eta\right)\cos^4(\phi_0)\\
&+\left(8\eta^8-1304\eta^6-1984\eta^4-384\eta^2\right)\cos^5(\phi_0)\\
&+\left(88\eta^7+64\eta^5+384\eta^3\right)\cos^6(\phi_0)\\
&\left.+\left(8\eta^8+128\eta^6+384\eta^4\right)\cos^7(\phi_0)\right)\\
\beta_5^s(\eta,\phi_0)&=\left(507\eta^6+1560\eta^4+1424\eta^2+384\right)\cos(\phi_0)\\
&+\left(1144\eta^5+2240\eta^3+896\eta\right)\cos^2(\phi_0)\\
&-\left(52\eta^6-384\eta^4-320\eta^2\right)\cos^3(\phi_0)\\
&-\left(64\eta^5+256\eta^3\right)\cos^4(\phi_0),
\end{aligned}\tag{100}$$

$$\begin{aligned}
\beta_1^h(\eta,\phi_0)&=4(1+\eta)\left(\left(27\eta^4+34\eta^2+8\right)\cos^2(\phi_0)\right.\\
&\left.+\left(20\eta^3+8\eta\right)\cos^3(\phi_0)-\left(2\eta^4+4\eta^2\right)\cos^4(\phi_0)\right),\\
\beta_2^h(\eta,\phi_0)&=-4\left(30\eta^5+44\eta^3+16\eta\right.\\
&+\left(75\eta^6+194\eta^4+144\eta^2+32\right)\cos(\phi_0)\\
&+\left(90\eta^5+132\eta^3+48\eta\right)\cos^2(\phi_0)\\
&\left.+\left(24\eta^4+16\eta^2\right)\cos^3(\phi_0)\right),\\
\beta_3^h(\eta,\phi_0)&=\frac{1}{1+\eta\cos(\phi_0)}\\
&\times\left(\left(210\eta^7+320\eta^5-344\eta^3-288\eta\right)\sin(\phi_0)\right.
\end{aligned}$$

$$
\begin{aligned}
&+\left(93\eta^6+18\eta^4-160\eta^2-64\right)\sin\left(2\phi_0\right)\\
&-\left(210\eta^7+344\eta^5-264\eta^3-224\eta\right)\sin^3\left(\phi_0\right)\\
&+\left(188\eta^6-80\eta^4-144\eta^2\right)\sin\left(\phi_0\right)\cos^3\left(\phi_0\right)\\
&-\left(40\eta^7+80\eta^5+64\eta^3\right)\sin\left(\phi_0\right)\cos^4\left(\phi_0\right)\\
&-\left(8\eta^6+16\eta^4\right)\sin\left(\phi_0\right)\cos^5\left(\phi_0\right)\Big),\\
\beta_4^h\left(\eta,\phi_0\right)&=\frac{1}{\left(1+\eta\cos\left(\phi_0\right)\right)^2}\\
&\Big(96\eta^5+96\eta^3+\left(-27\eta^6+4\eta^4-100\eta^2-48\right)\cos\left(\phi_0\right)\\
&-\left(342\eta^7+760\eta^5+616\eta^3+160\eta\right)\cos^2\left(\phi_0\right)\\
&-\left(219\eta^8+1158\eta^6+1356\eta^4+440\eta^2\right)\cos^3\left(\phi_0\right)\\
&-\left(500\eta^7+1260\eta^5+704\eta^3+48\eta\right)\cos^4\left(\phi_0\right)\\
&+\left(-10\eta^8-412\eta^6-456\eta^4-48\eta^2\right)\cos^5\left(\phi_0\right)\\
&+\left(12\eta^7-48\eta^5+48\eta^3\right)\cos^6\left(\phi_0\right)\\
&+\left(4\eta^8+32\eta^6+48\eta^4\right)\cos^7\left(\phi_0\right)\Big)\\
\beta_5^h\left(\eta,\phi_0\right)&=\left(243\eta^6+468\eta^4+276\eta^2+48\right)\cos\left(\phi_0\right)\\
&+\left(396\eta^5+464\eta^3+112\eta\right)\cos^2\left(\phi_0\right)\\
&-\left(18\eta^6-112\eta^4-40\eta^2\right)\cos^3\left(\phi_0\right)\\
&-\left(16\eta^5+32\eta^3\right)\cos^4\left(\phi_0\right).
\end{aligned}
\tag{101}
$$

References

1. Bloch, A.M., Marsden, J.E., Zenkov, D.V.: Nonholonomic dynamics. Not. AMS **52**(3), 324–333 (2005)
2. Ferrers, N.M.: Extension of Lagrange's equations. Q. J. Pure Appl. Math. **12**(45), 1–5 (1872)
3. Voronets, P.V.: On the equations of motion for nonholonomic systems. Mat. Sb **22**(4), 681–697 (1901)
4. Chaplygin, S.A.: Analysis of the Dynamics of Nonholonomic Systems. Classical Natural Sciences, Moscow (1949)
5. Chaplygin, S.A.: Selected works on mechanics and mathematics. State Publ. House, Technical-Theoretical Literature, Moscow (1954)
6. Hertz, H.: Die Prinzipien der Mechanik: in neuem Zusammenhange dargestellt, vol. 3. JA Barth (1910)
7. Borisov, A.V., Mamaev, I.S.: On the history of the development of the nonholonomic dynamics. arxiv:nlin/0502040 (2005)
8. De Leon, M.: A historical review on nonholomic mechanics. Revista de la Real Academia de Ciencias Exactas, Fisicas y Naturales Serie A. Matematicas **106**(1), 191–224 (2012)
9. Euler, L.: De minimis oscillationibus corporum tam rigidorum quam exililium, methodus nova et facilis. Commentarii Academiae Scientiarum Imperialis Petropolitanae **7**, 99–122 (1734)
10. Poisson, S.-D.: A treatise of mechanics, vol. 2. Longman and Company (1842)
11. Slesser, G.M.: Notes on rigid dynamics. Q. J. Math. **4**, 6567 (1861)
12. Vierkandt, A.: On sliding and rolling motion. Monatshefte der Mathematik and Physik, 3:31–54 and 97–134 (in German) (1892)
13. Chaplygin, S.A.: On a motion of a heavy body of revolution on a horizontal plane. Regul. Chaotic Dyn. **7**(2), 119–130 (2002)
14. Appell, P.: Sur l'intégration des équations du mouvement d'un corps pesant de révolution roulant par une arête circulaire sur un plan horizontal; cas particulier du cerceau. Rendiconti del Circolo Matematico di Palermo **14**, 1–6 (1900)
15. Korteweg, D.: Extrait d'une lettre 'a m.appel. Rendiconti del Circolo Matematico di Palermo **14**, 7–8 (1900)
16. Gallop, E.G.: On the rise of a spinning top. Trans. Camb. Philos. Soc. **19**, 356–373 (1904)
17. Carvallo, M.E.: Theory of motion of a monocycle and a bicycle: part 1. Hoop and monocycle, vol. 5 (1900)
18. Routh, E.J.: The Advanced Part of A Treatise on the Dynamics of a System of Rigid Bodies: Being Part II of a Treatise on the Whole Subject, vol. 229. Dover Publications, New York (1905)
19. Mindlin, I.M.: On the stability of motion of a heavy body of revolution on a horizontal plane, vol. 4 (1964)
20. Mindlin, I.M., Pozharitskii, G.K.: On the stability of steady motions of a heavy body of revolution on an absolutely rough horizontal plane. J. Appl. Math. Mech. **29**(4), 879–883 (1965)
21. Duvakin, A.P.: On the stability of motions of a disk, vol. 5 (1965)
22. Karapetyan, A.V., Rumyantsev, V.V.: Stability of conservative and dissipative systems. Itogi Nauki Tekh. Ser. Obshch. Mekh **6** (1983)
23. Kolesnikov, S.N.: Rolling of a disk along a horizontal plane. Vestnik Moskovskogo Universiteta. Seriya 1. Matematika. Mekhanika **2**, 55–60 (1985)
24. Fedorov, Y.N.: On disk rolling on absolutely rough surface. Izv. Akad. Nauk SSSR. Mekh. Tverd. Tela **4**, 67–75 (1987)
25. Kozlov, V.V.: On motion of disk on an inclined plain. Proc. Russ. Acad. Sci. Rigid Body Mech. **5**, 29–35 (1996)
26. O'reilly, O.M.: The dynamies of rolling disks and sliding disks. Nonlinear Dyn. **10**(3), 287–305 (1996)
27. Cushman, R., Hermans, J., Kemppainen, D.: The rolling disc. In: Nonlinear Dynamical Systems and Chaos, pp. 21–60. Springer (1996)
28. Kuleshov, A.S.: On stationary rollings of disk on rough surface. Appl. Math. Mech. **65**(1), 173–175 (2001)
29. Borisov, A.V., Mamaev, I.S., Kilin, A.A.: Dynamics of rolling disk. Regul. Chaotic Dyn. **8**(2), 201–212 (2003)
30. Zenkov, D.V., Bloch, A.M., Marsden, J.E.: The energy-momentum method for the stability of non-holonomic systems. Dyn. Stab. Syst. **13**(2), 123–165 (1998)
31. Paris, P.C., Zhang, L.: A disk rolling on a horizontal surface without slip. Math. Comput. Model. **36**(7–8), 855–860 (2002)

32. Cushman, R.H., Duistermaat, H., Sniatycki, J.: Geometry of Nonholonomically Constrained Systems, vol. 26. World Scientific, Singapore (2009)
33. Przybylska, M., Rauch-Wojciechowski, S.: Dynamics of a rolling and sliding disk in a plane. Asymptotic solutions, stability and numerical simulations. Regul. Chaotic Dyn. **21**(2), 204–231 (2016)
34. Kilin, A.A., Pivovarova, E.N.: Dynamics of an unbalanced disk with a single nonholonomic constraint. Regul. Chaotic Dyn. **28**(1), 78–106 (2023)
35. Borisov, A.V., Mamaev, I.S.: The rolling motion of a rigid body on a plane and a sphere. Hierarchy of dynamics. Regul. Chaotic Dyn. **7**(2), 177–200 (2002)
36. Hermans, J.: A symmetric sphere rolling on a surface. Nonlinearity **8**(4), 493 (1995)
37. Borisov, A.V., Mamaev, I.S., Bizyaev, I.A.: The hierarchy of dynamics of a rigid body rolling without slipping and spinning on a plane and a sphere. Regul. Chaotic Dyn. **18**(3), 277–328 (2013)
38. Borisov, A.V., Mamaev, I.S., Kilin, A.A.: The rolling motion of a ball on a surface. New integrals and hierarchy of dynamics. arxiv:nlin/0303024 (2003)
39. Borisov, A.V., Mamaev, I., Bizyaev, I., et al.: The Jacobi integral in nonholonomic mechanics. Regul. Chaotic Dyn. **20**(3), 383–400 (2015)
40. Borisov, A.V., Ivanova, T.B., Karavaev, Y.L., Mamaev, I.S.: Theoretical and experimental investigations of the rolling of a ball on a rotating plane (turntable). Eur. J. Phys. **39**(6), 065001 (2018)
41. Antali, M., Stepan, G.: Slipping-rolling transitions of a body with two contact points. Nonlinear Dyn. **107**(2), 1511–1528 (2022)
42. Hauser, J., Saccon, A.: The driven rolling torus. IFAC Proc. Vol. **40**(12), 101–106 (2007)
43. Agúndez, A.G., García-Vallejo, D., Freire, E.: Linear stability analysis of nonholonomic multibody systems. Int. J. Mech. Sci. **198**, 106392 (2021)
44. Schwab, A.L., Meijaard, J.P., Kooijman, J.D.G.: Some recent developments in bicycle dynamics. In: Proceedings of the 12th World Congress in Mechanism and Machine Science, pp. 1–6. Russian Academy of Sciences Moscow, Russia (2007)
45. Sharp, R.S.: On the stability and control of the bicycle. Appl. Mech. Rev. **61**(6), 060803 (2008)
46. Saccon, A., Hauser, J., Beghi, A.: A virtual rider for motorcycles: maneuver regulation of a multi-body vehicle model. IEEE Trans. Control Syst. Technol. **21**(2), 332–346 (2012)
47. Agúndez, A.G., García-Vallejo, D., Freire, E.: Linear stability analysis of a bicycle multibody model with toroidal wheels. In: Advances in Nonlinear Dynamics, pp. 477–487. Springer (2022)
48. Agúndez, A.G., García-Vallejo, D., Freire, E., Mikkola, A.: A reduced and linearized high fidelity waveboard multibody model for stability analysis. J. Comput. Nonlinear Dyn. **17**(5), 051010 (2022)
49. García-Agúndez, A., García-Vallejo, D., Freire, E.: Linearization approaches for general multibody systems validated through stability analysis of a benchmark bicycle model. Nonlinear Dyn. **103**, 1–24 (2021)
50. Schiehlen, W.: Multibody system dynamics: roots and perspectives. Multibody Syst. Dyn. **1**(2), 149–188 (1997)
51. Tatum, J.: Classical Mechanics. University of Victoria, Victoria (2013)
52. Voronetz, P.V.: Transformation of the equations of motion by means of linear integrals of motion (with an application to the n-body problem). Kiev. Univ. Izv. **47**(1–2), 192 (1907)
53. Koiller, J.: Reduction of some classical non-holonomic systems with symmetry. Arch. Ration. Mech. Anal. **118**(2), 113–148 (1992)
54. Borisov, A.V., Mamaev, I.S.: Symmetries and reduction in nonholonomic mechanics. Regul. Chaotic Dyn. **20**, 553–604 (2015)